# Modeling Sharp Wave-Ripple Complexes Through a CA3-CA1 Network Model with Chemical Synapses

Jiannis Taxidis,[1]* Stephen Coombes,[1] Robert Mason,[2] and Markus R. Owen[1]

**ABSTRACT:** The hippocampus, and particularly the CA3 and CA1 areas, exhibit a variety of oscillatory rhythms that span frequencies from the slow theta range (4–10 Hz) up to fast ripples (200 Hz). Various computational models of different complexities have been developed in an effort to simulate such population oscillations. Nevertheless the mechanism that underlies the so called Sharp Wave-Ripple complex (SPWR), observed in extracellular recordings in CA1, still remains elusive. We present here, the combination of two simple but realistic models of the rat CA3 and CA1 areas, connected together in a feedforward scheme mimicking Schaffer collaterals. Both network models are computationally simple one-dimensional arrays of excitatory and inhibitory populations interacting only via fast chemical synapses. Connectivity schemes and postsynaptic potentials are based on physiological data, yielding a realistic network topology. The CA3 model exhibits quasi-synchronous population bursts, which give rise to sharp wave-like deep depolarizations in the CA1 dendritic layer accompanied by transient field oscillations at ∼150–200 Hz in the somatic layer. The frequency and synchrony of these oscillations is based on interneuronal activity and fast-decaying recurrent inhibition in CA1. Pyramidal cell spikes are sparse and come from a subset of cells receiving stronger than average excitatory input from CA3. The model is shown to accurately reproduce a large number of basic characteristics of SPWRs and yields a new mechanism for the generation of ripples, offering an interpretation to a range of neurophysiological observations, such as the ripple disruption by halothane and the selective firing of pyramidal cells during ripples, which may have implications for memory consolidation during SPWRs. © 2011 Wiley-Liss, Inc.

KEY WORDS: ripples; sharp waves; hippocampal modeling; oscillations; synchrony

## INTRODUCTION

Sharp Wave-Ripple complexes (SPWRs) are a major characteristic pattern of hippocampal activity, appearing in electroencephalogram (EEG) and local field potential (LFP) recordings during deep sleep, anesthesia, awake rest, consummatory behavior and immobility, and disappearing during sensory stimulations (Buzsáki, 1986; Buzsáki et al., 1992).

The first component of the complex, the sharp wave, is characterized by a large negative peak in the EEG signal followed by a small positive one, with duration between 30 and 120 msec and frequency of occurrence between 0.01–3 Hz (Buzsáki, 1986). Sharp waves are located in the apical dendritic layer of the CA1 region where their amplitude reaches its maximum, and they reverse polarity above the pyramidal cell layer (Buzsáki, 1986; Ylinen et al., 1995; Maier et al., 2003). Various studies have shown that the source of sharp waves is synchronous population bursts in CA3 (Ylinen et al., 1995; Csicsvari et al., 2000; Maier et al., 2003) generated by its recurrent excitatory circuit (Miles and Wong, 1987; Traub et al., 1989). A barrage of excitatory currents, originating from such discharges, propagates through the Schaffer collaterals and results in an extensive depolarization of CA1 dendrites giving rise to a sharp wave (Buzsáki, 1986; Ylinen et al., 1995; Maier et al., 2003). These CA3 discharges activate not only CA1 pyramidal cells but interneurons as well, giving rise to transient oscillatory ripple patterns of ∼150–200 Hz frequency which constitute the second component of the SPWR (Buzsáki et al., 1992; Ylinen et al., 1995; Maier et al., 2003). Their current source is located in the CA1 pyramidal cell layer, where their amplitude is maximal and decreases sharply toward the strata radiatum and oriens (Ylinen et al., 1995; Maier et al., 2003). Ripples are characterized by a dramatic increase in the firing rates of both pyramidal cells and interneurons (Csicsvari et al., 1999) [basket cells in particular (Klausberger et al., 2003)] but individual neurons fire spikes at much lower frequencies, indicating that ripples do not reflect the activity of single cells but instead are a field rhythm involving both populations (Csicsvari et al., 1999; Maier et al., 2003).

An important feature of SPWRs is that they are very widespread, extending throughout the CA3-CA1-subiculum complex-enthorinal cortex axon, involving the synchronized participation of tens of thousands of cells (Chrobak and Buzsáki, 1996). This synchronous activity that quickly builds up during the ripples is not consistently initiated from the same site but emerges simultaneously from several locations (Ylinen et al., 1995). The strong transient output, produced during such massive population discharges, is very likely to affect neocortical targets, rendering SPWRs a possible means for memory transfer from the hippocampus to the neocortex for long-term storage, during

[1] Division of Applied Mathematics, University of Nottingham, Nottingham, United Kingdom; [2] Institute of Neurosciences, Queen's Medical Centre, University of Nottingham, Nottingham, United Kingdom

*Correspondence to: Jiannis Taxidis, Pope Building C9, School of Mathematical Sciences, University of Nottingham, NG7 2RD, Nottingham, UK. Email: pmxit@nottingham.ac.uk.

deep stages of sleep. Correlations between ripples and cortical slow oscillations during deep sleep (Siapas and Wilson, 1998; Sirota et al., 2003; Battaglia et al., 2004; Isomura et al., 2006) and the fast-scale replay, during SPWRs, of temporal patterns of correlated place cells in forward (Wilson and McNaughton, 1994; Skaggs and McNaughton, 1996; Lee and Wilson, 2002) or reversed order (Foster and Wilson, 2006; Diba and Buzsáki, 2007) support the role of SPWRs in memory consolidation.

Although SPWRs have been widely studied both *in vivo* (Buzsáki, 1986; Buzsáki et al., 1992; Ylinen et al., 1995; Chrobak and Buzsáki, 1996; Csicsvari et al., 1999, 2000; Klausberger et al., 2003) and *in vitro* (Maier et al., 2002, 2003; Behrens et al., 2005; Nimmrich et al., 2005; Wu et al., 2005; Both et al., 2008) in rats and mice, the mechanism that generates them still remains unclear. Sparse networks of CA1 pyramidal cells coupled together with axo-axonal gap junctions have been proposed to underlying high frequency hippocampal oscillations (Draguhn et al., 1998; Schmitz et al., 2001). Indeed, computational models of such networks (Traub et al., 1999b) or with inclusion of interneurons and synaptic interactions as well (Traub and Bibbig, 2000), have been shown to give rise to ripple-like ~200 Hz population oscillations. This proposed mechanism is supported by the suppression of ripples under gap-junction blockers (Ylinen et al., 1995; Maier et al., 2003) but contradicted by lack of SPWR generation from antidromic stimulation of CA1 pyramidal axons and by preservation of SPWRs after removal of the distal part of these axons (Both et al., 2008).

Another suggested mechanism involves the cross-talk between pyramidal cells and interneurons. It has been proposed that the excitatory barrage by the discharging CA3 and CA1 pyramidal neurons results in a relatively steady depolarization of the target interneurons causing fast rhythmic oscillation of their membrane potential and sustained firing. When a critical number of spatially distributed interneurons fires at ~200 Hz, they will coordinate the firing of their pyramidal cell targets, which in turn will phase reset the next firing of their interneuronal contacts. Thus spatially distributed synchrony could be quickly established through pyramidal–interneuron interactions (Buzsáki et al., 1992; Ylinen et al., 1995; Csicsvari et al., 1999). It is noteworthy that the involvement of fast perisomatic inhibition was recently shown to be critical for the *in vitro* generation of SPWRs in CA3 slices (Ellender et al., 2010).

We present here, the combination of two simple but physiologically realistic computational models of the rat CA3 and CA1 areas, respectively. The CA3 model is characterized by long-range recurrent excitatory connections and the CA1 by a strong inhibitory network, while both models include connections between excitatory and inhibitory populations. The two models are initially explored separately and are shown to successfully reproduce a range of anatomical characteristics and/or functional properties of the corresponding hippocampal areas. The CA3 model, due to recurrent excitation combined with strong inhibition, exhibits quasi-synchronous population bursts that are theta-periodic (4–10 Hz) while the CA1 model produces population oscillations that lie in the gamma frequency range (40–100 Hz) or above it. The two models are coupled

together in a feed-forward fashion with excitatory connections from CA3 to CA1 that mimic Schaffer collaterals. The full CA3-CA1 network exhibits synchronized oscillatory ~150–200 Hz responses in CA1 to excitatory input from CA3 population bursts. We show that these responses closely resemble SPWRs and share a large number of the characteristic features reported through various neurophysiological recordings.

To the best of our knowledge, our full CA3-CA1 network offers a novel approach to SPWR modeling and suggests a different version of the pyramidal-interneuron interaction mechanism for ripple generation. The widespread Schaffer collateral connections generate an almost homogeneous depolarizing input to pyramidal cell dendrites and to fast spiking interneurons in CA1, giving rise to a sharp wave. This depolarization would drive isolated interneurons to intrinsically spike at a wide range of high frequencies (~100–400 Hz). Strong and fast-decaying inhibition between interneurons contains their firing within the range of ripple frequencies (~150–200 Hz) and helps in the synchronization of their oscillation over hundreds of μm. Pyramidal cells are more passive since the synchronized inhibitory barrage they receive during the ripple, cancels on average the depolarization from CA3. A minority of cells, receiving stronger input from CA3 than the rest, produces the majority of excitatory spikes.

## METHODS

### General Model Architecture and Single Cell Models

The two models represent the CA3 and CA1 rat hippocampal areas respectively, in the longitudinal direction. They are one-dimensional arrays containing 1000 pyramidal cells and 100 interneurons, keeping the ratio of 10:1 pyramidal cells-to-interneurons that has been estimated for the hippocampus (Traub and Miles, 1991; Andersen et al., 2006). The intercellular distance was set to 10 μm in both cases, yielding a total length 11 mm, close to the 10 mm length of a longitudinal CA3 slice (Traub and Miles, 1991). The interneurons are equidistantly distributed among the pyramidal cells, with one interneuron every ten cells. The total surface area of each pyramidal cell is set to 50,000 μm², close to the 50,400 μm² reported for CA3 cells (Cannon et al., 1999) but a slight overestimate for CA1 cells with 36,000 μm² surfaces (Cannon et al., 1999). The total surface area of each interneuron is set to 20,000 μm², close to the 12,000 μm² for dentate gyrus basket cells reported by (Bartos et al., 2001). The two arrays are considered parallel and the distance between them was set to 100 μm.

Pyramidal cells are modeled by the two-compartmental Pinsky-Rinzel model (Pinsky and Rinzel, 1994), which closely reproduces the various firing properties of hippocampal cells. The parameter values are taken from the original model with the only exception being the $Ca^{2+}$ maximum conductance $g_{Ca^{2+}}$ for the CA1 pyramidal cells, which was reduced to 7 mS/cm² (from 10 mS/cm²). This was done to simulate better the *in vitro*

characteristic firing properties of such cells, where the typical CA3 intrinsic bursting is replaced by tonic firing with frequency accommodation (Madison and Nicoll, 1984; Andersen et al., 2006). When depolarizing these modified Pinsky-Rinzel model neurons with low currents, in the somatic compartment, they also exhibit tonic firing with a frequency that quickly attenuates to a constant value. Higher currents result in an initial burst that is followed by accommodating tonic firing. Their firing rate increases linearly with increasing current and the accommodation becomes faster. The slope of the f–I curve, calculated through the last interspike interval after a 2 sec run, is approximately 30.35 Hz/nA which is in good agreement with the 34.1 Hz/nA slope estimated through single cell recordings (Lanthorn et al., 1984).

Although many different types of interneurons exist in the hippocampus (Freund and Buzsáki, 1996; Cutsuridis et al., 2010a,b), all interneurons here are considered to be perisomatic basket cells, i.e. targeting only the axosomatic compartment of pyramidal cells. In contrast, all excitatory connections target their dendritic compartment. Interneurons are modeled by the Wang-Buzsáki model (Wang and Buzsáki, 1996), a very simple single-compartment model that accurately captures the firing properties of fast spiking basket cells.

Heterogeneity in the system is added by varying the reversal potential and the maximum conductance of the leakage current throughout the network. These are distributed over the cells according to a Gaussian distribution centered on the value for the corresponding single cell model with standard deviation (SD) equal to 0.5% of that value. Additionally, the maximum conductance of the coupling current between the two compartments of the Pinsky-Rinzel model is varied in pyramidal cells following the same scheme.

The initial conditions in all simulations were also Gaussian-distributed over both pyramidal and interneuronal populations. The means of the distributions were equal to the steady states of the corresponding single cell models. Their SD was 10% in all cases.

## Synaptic Interactions

Only fast AMPA and GABA$_A$-mediated synaptic interactions are considered in both models, with synaptic currents given by:

$$I_{syn} = \bar{g}_{syn} s_{syn}(V - V_{syn}) \quad (1)$$

where $\bar{g}_{syn}$ is the maximum conductance, $V$ is the membrane potential of the postsynaptic cell, $V_{syn}$ is the reversal potential of the synapse and $s_{syn}$ is an exponentially decreasing gating variable:

$$\frac{ds_{syn}}{dt} = -\frac{s_{syn}}{\tau_{syn}} \quad (2)$$

with $\tau_{syn}$ the decay constant. When an action potential arrives at a synapse, $s_{syn}$ in the postsynaptic cell is increased by a fixed value $\alpha_{syn}$. For simplicity, we have set $\bar{g}_{syn} = 1nS$ for all synapses, so that the postsynaptic potential (PSP) amplitudes are controlled by $\alpha_{syn}$. The values of $\alpha_{syn}$ for all types of synapses are given in Table 1, along with the PSPs they yield and the corresponding

**TABLE 1.**

*Synaptic Parameters*

|  |  | $\alpha_{syn}$ | PSP (mV) | Reported PSP (mV) | Reference |
|---|---|---|---|---|---|
| CA3 | PY-PY | 15 | 1 | 0.6–1.3 | Miles and Wong (1986) |
|  | PY-IN | 3 | 1.6 | 1.9 | Miles (1990) |
|  | IN-PY | 50 | 1.2 | 1.2 | Miles et al. (1996) |
| CA1 | PY-IN | 2.5 | 1.3 | 1.4 | Ali et al. (1998) |
|  | IN-PY | 15 | 0.5 | 0.45 | Buhl et al. (1995) |
|  | IN-IN | 5 | 0.5 | 0.25 | Cobb et al. (1997) |
| Schaffer | PY-PY | 1.5 | 0.13 | 0.13 | Sayer et al. (1990) |
|  | PY-IN | 0.8 | 0.4 |  |  |

Parameter values for the synaptic strength of all types of synapses in the full model along with the resulting PSPs and the ones reported through physiological recordings. All PSPs in the model were measured from a background membrane potential of $-65.3$ mV for CA3 pyramidal cells, $-62.6$ mV for CA1 pyramidal cells and $-62$ mV for all interneurons.

recorded PSPs that were used as reference. Note that only the inhibitory PSPs (IPSPs) on CA1 interneurons deviate from the cited value because in these particular connections we replicated the 5 nS peak conductance reported by Bartos et al. (2002). Since, to our knowledge, there have been no reported values for Schaffer collateral excitatory PSPs (EPSPs) on CA1 interneurons, we arbitrarily set the EPSP to 0.4 mV. This gives a ratio of Schaffer collaterals' EPSPs to EPSPs from CA1 pyramidal cells equal to 0.4/1.4 = 28%. This is comparable to the corresponding ratio for CA1 pyramidal cells which is roughly 0.13/0.7 = 19% (given an average EPSP amplitude between CA1 pyramidal cells of roughly 0.7 mV (Deuchars and Thomson, 1996).

The AMPA decay time constant is set to 2 msec (Geiger et al., 1995). Importantly, for GABA$_A$ synapses between interneurons we set an equally short time constant of 2 msec, following Bartos et al. (2002, 2007). For GABA$_A$ synapses targeting pyramidal cells the decay time constant was set to 7 msec which is between the ˜4 msec reported by Bartos et al. (2002) and the 10 msec time constant usually implemented in similar simulations (Wang and Buzsáki, 1996; Traub et al., 1996a, 1999b).

The conduction velocity of the CA3 pyramidal cell axon has been shown to be approximately 0.5 mm/msec (Miles et al., 1988). We use this velocity in both our CA3 and CA1 model. The corresponding velocity for CA1 interneurons was set to 0.1 m/s (Salin and Prince, 1996). We treat propagation over CA3 interneuronal axons as instantaneous.

## General Connectivity

The CA3 model is characterized by many recurrent excitatory connections while connections between CA3 interneurons are omitted. The opposite holds for CA1 where interneurons are strongly connected with each other while recurrent excitatory connections are absent.

The connectivity scheme in both models is similar and follows one applied in a cortical model by Compte et al., (2003). The number of connections from cells of type $i$ to cells of type $j$, where $i$ and $j$ can stand for pyramidal cells or interneurons, are drawn from a Gaussian distribution with mean $k_{ij}$ and standard deviation $k_{ij}/20$. The assigned connections are distributed to the $j$-cells according to a gaussian probability distribution, centered on the source cell, with a fixed SD equal to $\sigma_i$:

$$P(x) = \frac{e^{-x^2/2\sigma_i^2}}{\sqrt{2\pi\sigma_i^2}} \tag{3}$$

where $x$ is the distance of each $j$-cell from the source cell. In both CA3 and CA1 models, all excitatory connections have a SD of $\sigma_{PY} = 1$ mm $= 100$ cells while interneurons have $\sigma_{IN} = 100$ µm $= 10$ cells. Multiple connections are allowed but not autapses.

Our connectivity scheme means that the further away a cell is from the source, the smaller the probability that it will get connected. The only exception to this scheme was connections from CA3 interneurons to CA3 pyramidal cells, for which all connections were uniformly distributed around each interneuron to cells within distance $3\sigma_{IN}$.

According to the empirical rule for the Gaussian distribution, 99.7% of the distributed connections will lie within a distance of $3\sigma_i$ from the source cell. Therefore almost all connections are expected to be distributed to cells within a "connectivity cluster" of total size $6\sigma_i$. For example, the pyramidal-pyramidal connections in CA3 can reach out to distances of $3\sigma_{PY} = 3$ mm covering 600 cells. These clusters are in broad agreement with neurophysiological recordings. For recurrent excitatory connections in CA3, it has been shown that *in vivo* CA3 axons can extend at least one-half the length of the hippocampus in the longitudinal direction (Traub et al., 1999a) but that the probability of synaptic contact between two pyramidal cells drops as a function of their distance, reaching out to 3–5 mm (Miles et al., 1988; Traub and Miles, 1991).

In practice, the $i$-to-$j$ connectivity cluster will be smaller than $6\sigma_i$, since cells of the opposite type of $j$ will also lie within it and since the closer the source cell is to the array boundaries the fewer the available cells. Moreover, multiple connections in the case of small clusters may result in the average number of contacted cells being reduced from $k_{ij}$ to a value $\tilde{k}_{ij}$. The connectivity probability between any pair of cell types is estimated as the average number of contacted cells $\tilde{k}_{ij}$ over the average cluster size.

The implemented average number of connections along with the average number of contacted cells $\tilde{k}_{ij}$ is summarized in Table 2 for every pair of cell types. The average cluster sizes (estimated through 20 repetitions of the connectivity algorithms) and the corresponding connectivity probabilities are also listed. A schematic diagram of the model is illustrated in Figure 1A, along with an example of the connectivity matrix of pyramidal-pyramidal connections in CA3 (Fig. 1C).

TABLE 2.

*Connectivity Parameters*

| | | Average Cluster Size | $k_{ij}$ | $\tilde{k}_{ij}$ | Connectivity probability |
|---|---|---|---|---|---|
| CA3 | PY-PY | 471.77 | 55 | 50.1 | 10.62% |
| | PY-IN | 47.15 | 5 | 4.66 | 9.88% |
| | IN-PY | 55.2 | 68 | 39.16 | 71.3% |
| CA1 | PY-IN | 47.15 | 20 | 14.67 | 31.11% |
| | IN-PY | 55.2 | 400 | 46.35 | 83.97% |
| | IN-IN | 4.94 | 100 | 4.49 | 90.89% |
| Schaffer | PY-PY | 548.02 | 130 | 99.81 | 18.21% |
| | PY-IN | 54.84 | | 10.01 | 18.25% |

Connectivity parameter values for every connected pair of cell types. The average cluster size is the number of target cells within a distance of $3\sigma_j$ from an average neuron, $k_{ij}$ is the average number of connections each cell makes with the target cells while $\tilde{k}_{ij}$ is the average number of different cells it contacts.

## CA3 Connectivity

The average number of connections a CA3 pyramidal cell makes was set to 190. Of these, 97.4% = 185 connections target other pyramidal cells and the remaining 2.6% = 5 connections target CA3 interneurons, in accordance with the observation that ~2.1% of the boutons of a studied CA3 pyramidal cell targeted parvalbumin-positive interneurons (Sik et al., 1993). It has also been estimated that most of the pyramidal cells each CA3 cell contacts are located in the CA1 area, the rest forming recurrent excitatory connections within CA3 (Li et al., 1994; Traub et al., 1999a). Accordingly, the 185 connections targeting other pyramidal cells in the model are further divided into 70% = 130 that form Schaffer collaterals to CA1 while the remaining 30% = 55 connections target other pyramidal cells within CA3.

Pair recordings of pyramidal cells in transverse CA3 slices indicate that the probability two such cells are connected is roughly 2% (MacVicar and Dudek, 1980). However, it has been argued that the actual probability inside the intact CA3, in the longitudinal direction, can be much higher, even up to 15% (Bernard and Wheal, 1994). The connectivity probability in our model is on average 10.62%, well within the estimated limit for the intact CA3.

The average cluster size of CA3 pyramidal-to-interneuron connections is approximately 47 cells. Since this cluster is large enough for the 5 distributed connections, very few polysynaptic connections arise ($\tilde{k}_{PY-IN} = 4.66$), in accordance with the observation that excitatory connections to interneurons are mostly monosynaptic (Traub et al., 1999a). Moreover, the estimated probability of finding a pyramidal-to-interneuron connection within a transverse CA3 slice is about 10% (Miles et al., 1988; Traub and Miles, 1991). Similarly, the corresponding probability in our model is 9.88%.

The interneuronal axons deviate widely in a transverse CA3 slice but their outputs extend only to around 300 µm (Bernard and Wheal, 1994; Traub et al., 1999a). In a series of CA3
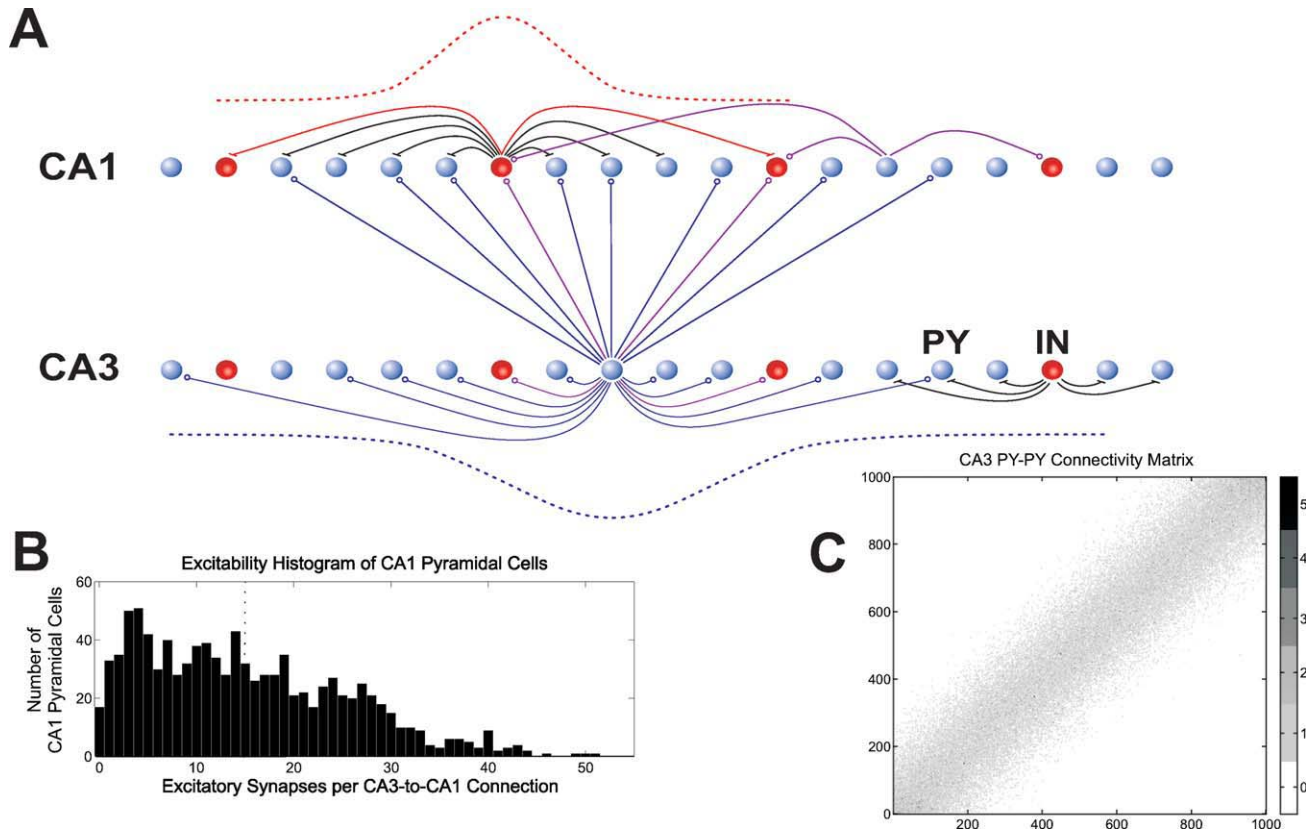
FIGURE 1. A: Schematic diagram of the full CA3-CA1 model. The bottom array represents CA3 and the top CA1. The light (blue) spheres are pyramidal cells and the dark (red) ones are interneurons (1:4 cell ratio is shown for clarity, instead of the real 1:10). A qualitative picture of the connectivity is illustrated through four example cells. The two gaussian distributions represent the connectivity probability as a function of distance from a pyramidal cell (bottom) and an interneuron (top). B: Histogram of the synapses-per-Schaffer collateral connection of CA1 pyramidal cells. The dotted line represents the mean of the distribution (15 synapses). C: Connectivity matrix of the pyramidal-to-pyramidal connections in CA3. The color scale represents the amount of multiple connections. [Color figure can be viewed in the online issue, which is available at wileyonlinelibrary.com.]

computational models (Traub and Miles, 1991; Traub et al., 1992), the numbers of interneuronal outputs are tenfold the pyramidal ones but excitatory connections are 5 times more extensive. In our model, each interneuron has 68 connections on average, distributed uniformly around the cell over a maximum distance of $3\sigma_{IN} = 300$ μm. Hence excitatory connections are 10 times more extensive than inhibitory ones. As expected, many polysynaptic connections arise ($\tilde{k}_{IN-PY} = 39.16$) in accordance with the observation that perisomatic interneurons form multiple connections on each pyramidal cell (Traub et al., 1999a). The resulting connection probability is approximately 71.3%, close to the estimated 60% in slices (Miles et al., 1988; Traub and Miles, 1991).

We counted the number of pyramidal cells reached through excitatory connections, monosynaptically, disynaptically, and trisynaptically from a pyramidal cell in the middle of the array. The particular cell contacts 4.4% of all cells directly, 59.3% through two steps and 99.7% through three steps. We also counted the pyramidal cells that are inhibited by the previous central pyramidal cell through one intermediate interneuron (one step), those that are inhibited by the interneurons contacted by its pyramidal connections (two steps) and so on. We

found that 12.3% of all pyramidal cells are inhibited through one step, 67.9% through two and 99.7% through three steps. Therefore, virtually the whole network can be reached within three excitatory connections from a central pyramidal cell or can be indirectly inhibited by its activity. Both these features are in agreement with the two dimensional CA3 model by Traub et al. that accurately reproduces a large number of CA3 features [see Figures 5.4 and 5.6 in Traub and Miles (1991)].

## CA1 Connectivity

Connectivity in CA1 is more loosely based on anatomical data and more focused on reproducing features of the intrinsic CA1 gamma oscillations through a strongly interconnected inhibitory network.

The extent of pyramidal connections is the same as in CA3, but now they are set to target only interneurons, since various studies have shown that there is a distinct preference for CA1 pyramidal cells to target interneurons while recurrent excitation is very sparse (Andersen et al., 2006). The connection probability from pyramidal cells to stratum pyramidale interneurons was calculated to be roughly 30% (Knowles and Schwartzkroin,

1981). Although different interneuronal subclasses have been shown to have different probabilities of receiving excitatory inputs, we chose to follow the general stratum pyramidale estimate, by setting $k_{\text{PY-IN}} = 20$, which yields a connection probability of 31.11%. Since the actual average number of interneurons targeted by each pyramidal cell is $\hat{k}_{\text{PY-IN}} = 14.67$, few polysynaptic connections arise, again in agreement with pair recordings (Gulyás et al., 1993a).

Unlike the relatively few excitatory connections, interneurons form many polysynaptic connections to neighboring cells. Basket cell axons in CA1 were found to generally span less than 1 mm (Sik et al., 1995). In a CA1 modeling study this span was set to 500 µm (Traub et al., 1999c). In our model, the corresponding span is of the same order and can reach 300 µm. Furthermore, the CA1 basket-to-pyramidal cell connection probability was found to be roughly 30%, dropping abruptly with distance from the soma, from 54% for immediate neighbors to 5% for distant ones (Knowles and Schwartzkroin, 1981; Andersen et al., 2006). In the model, the average connection probability is larger, at 83.97%. Nevertheless, it yields that the average number of contacts each interneuron makes on a pyramidal cell is 8.54 with the corresponding estimated average being 6 contacts (Gulyás et al., 1993b; Buhl et al., 1994).

Although little information is available on the characteristics of recurrent inhibitory connections in CA1, it is established through *in vitro* pair recordings in slices that basket cells are highly interconnected (Bartos et al., 2007) with each basket cell contacting at least 60 others (Sik et al., 1995). We have set an average of 100 connections each interneuron makes to others, but the fact that they are equidistantly distributed on the array, 110 µm apart, yields a very small connectivity cluster (∼5 cells), and consequently a very high connection probability of 90.89% within the cluster.

## Schaffer Collateral Connectivity

Schaffer collaterals are the major input to CA1 pyramidal cells with each CA3 pyramidal cell contacting 30,000–60,000 cells and its axonal projections extending to more than two thirds the length of CA1 (Li et al., 1994). Schaffer collaterals are expected to excite CA1 interneurons as well, although to our knowledge the characteristics of such connections have not been studied yet.

We connect the two CA models in a feedforward fashion with each CA3 pyramidal cell contacting 130 CA1 neurons on average (see also section on CA3 connectivity). Similar to the previous connectivity scheme, the Schaffer collateral connections of each CA3 cell are distributed according to a Gaussian probability distribution centered on the corresponding pyramidal cell in CA1. However, the connections are distributed in CA1 irrespective of whether the contacted cell is pyramidal or interneuron. The SD was set to $\sigma_{\text{CA3-CA1}} = 1.2$ mm, so that connectivity clusters can reach 7.2 mm in size, roughly two thirds the total extent of the array.

Consequently, each CA1 cell receives weak input from approximately 100 CA3 pyramidal cells, which is a great underestimate of the total amount of excitation each cell is expected to receive from CA3 (Andersen et al., 2006). To counterbalance the small number of pyramidal cells in our CA3 array and have the necessary strong input in CA1 we assign multiple synapses to each CA3-to-CA1 connection. Although, to our knowledge, the number of contacts between a CA3 and CA1 pyramidal cell have not been thoroughly studied [see Andersen et al. (2006) for an analysis of the difficulty of such a task], it has been estimated that it lies between two to ten contacts (Sorra and Harris, 1993). For each CA1 interneuron we fix the number of synapses it receives from each contact to 13. The corresponding number for the pyramidal cells varies. For each cell, it is drawn from a gaussian distribution: $13 \pm 13$ (mean ± SD). To avoid negative numbers, the absolute value of each drawn number is taken. This scheme results in most cells receiving relatively few synapses (∼15 on average) from each assigned CA3-to-CA1 connection. Nevertheless, a minority of pyramidal cells receives many more synapses than average, yielding a subset of pyramidal cells that will be driven by much stronger input from CA3 than the rest. These cells are assumed to represent real neurons in the rat CA1 that are targeted by a larger portion of CA3 or receive stronger EPSPs than average. The histogram of this heterogeneous 'excitability' is given in Figure 1B.

## Simulations of Extracellular Recordings

Most studies on SPWRs are made with depth-EEG and LFP recordings, detecting extracellular activity from an area around the tip of the electrode. To simulate such local activity recordings in CA1, we avoided storing data from the whole array and focused on a specific site of length 560 µm in the middle of the CA1 array, containing 50 pyramidal cells and 6 interneurons. We will refer to this as the 'default recording site' throughout the text.

We model extracellular synaptic activity using two similar measures: (1) the total post-synaptic currents $I_{\text{syn}}(t)$ and (2) the total conductances $\bar{g}_{\text{syn}} s_{\text{syn}}(t)$, summed over all synaptic connections over the whole recording site. The first measure was used to reproduce raw extracellular recordings visually and for the study of postsynaptic currents developing in the average cell during a SPWR. But since its definition contains the intracellular membrane potential of cells [Eq. (1)], it will be affected by any phase delays between population synaptic activity and membrane potential responses. Since the second measure takes only non-negative values it does not reproduce the raw recordings of an EEG or LFP probe visually, but is appropriate for fine timescale analysis since it will not be affected by any of the aforementioned delays. We will refer to these two measures as "total synaptic currents" and "total synaptic conductances" throughout the text.

To simulate CA1 dendritic layer and pyramidal cell layer recordings separately, the aforementioned measures are split into two components: (1) Dendritic layer recordings are assumed to correspond to the excitatory synaptic currents/conductances from Schaffer collaterals that act on the dendritic compartment of pyramidal cells and on the single-compartment interneurons
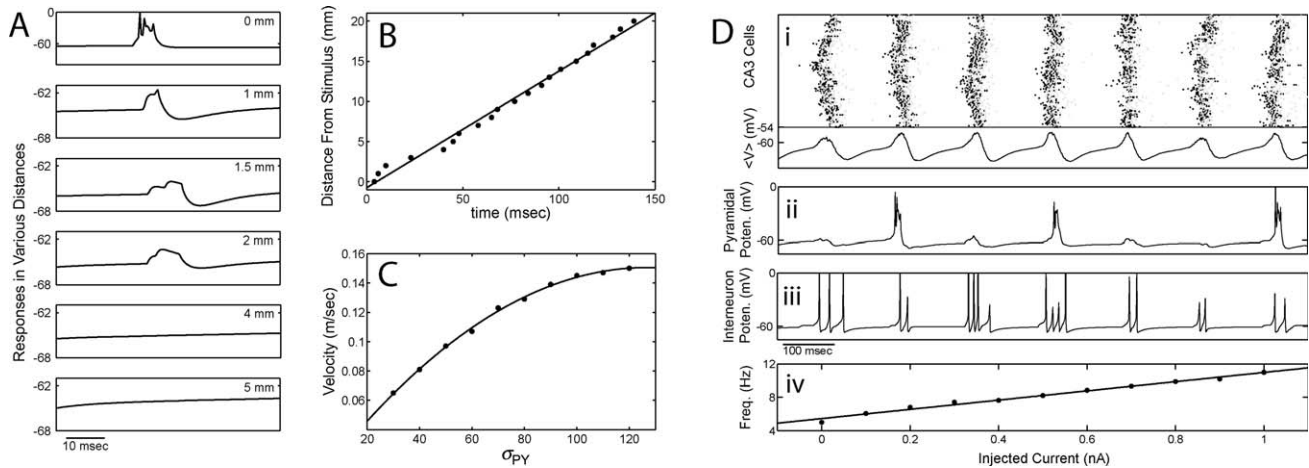
FIGURE 2.   A: Responses of pyramidal cells at different distances from a stimulation at one end of the CA3 array. The membrane potential of one of the stimulated cells is shown in the top panel. The other panels correspond to cells at different distances from the stimulation site. B: Distance from the stimulation at one end of the disinhibited CA3 array, against the time the propagating activity reaches that distance. The line represents the least squares fit and yields a propagation velocity of approximately 0.145 m/sec. C: The propagation velocity increases as a function of the extent of excitatory connections. D: Quasi-synchronous theta-frequency oscillations in the full CA3 model. Raster plot (pyramidal cell spikes are shown in black and interneuronal in gray) and average membrane potential of the whole model (a) Examples of membrane potentials from one pyramidal cell (b) and one interneuron (c). Some spikes have been truncated and others appear as spikelets due to the 1 kHz sampling frequency of membrane potentials. Relation between the frequency of the population bursts in CA3 and the depolarizing current, applied on the dendritic compartments of pyramidal cells (d). Note that even for zero current the oscillations are within the theta-frequency band.

[since the dendrites of basket cells lie in the CA1 dendritic layer (Freund and Buzsáki, 1996)]. (2) Somatic (pyramidal cell) layer recordings are assumed to correspond to synaptic currents/conductances from pyramidal-to-interneuron, interneuron-to-pyramidal and interneuron-to-interneuron connections.

### Ripple Detection

Ripples are detected from the 150–200 Hz bandpass filtered version of the total synaptic conductances of the somatic layer. The algorithm for their detection is the following: The root mean square (RMS) of the measure is calculated in non-overlapping bins of 10 msec duration. The SD of the RMS is derived over the whole signal. Ripples are detected when the RMS exceeds a $2 \times$ SD threshold. Their boundaries are set where the RMS drops below $1 \times$ SD around the ripple. Ripples with less than 20 msec total duration are discarded and neighboring ripples less than 10 msec apart are taken as one event. Similar algorithms were used by Csicsvari et al. (1999, 2000) and Klausberger et al. (2003).

In a typical 30 sec simulation, 170 ripple episodes are detected, with average duration of 61 msec [similar to the 50 msec duration in Ylinen et al. (1995)] with a range between 20–90 msec [30–80 msec in Maier et al. (2003)].

For the averaging over ripples, all detected events are aligned using the minimum point of the filtered signal as reference (point 0 msec).

### Numerical Methods

The model was implemented in the spiking neural networks simulator "Brian" in Python (www.briansimulator.org, Goodman and Brette, 2008), using a second-order Runge-Kutta method with a time step of 0.05 msec. Spikes are recorded at every time step, whereas all other variables are recorded at every 1 msec, yielding a maximum frequency of 500 Hz for spectral estimation. Analysis and plotting of results was performed with Brian and MATLAB.

## RESULTS

Before modeling SPWRs by the full CA3-CA1 model, we test the two individual models separately by reproducing a series of features observed in neurophysiological recordings or simulations of more sophisticated models. This was done in an effort to validate the two models by showing that they are realistic representations of the corresponding hippocampal areas and can reproduce some of their basic intrinsic characteristics and behaviors. These tests also give insight into the mechanism of SPWR generation by the full model.

### Population Bursts in the CA3 Model

To test the network's response to a stimulation at one end of the array we applied a depolarizing stimulus of 8 nA for 2 msec in the leftmost 10 cells of the array and recorded the membrane potentials of pyramidal cells lying at distances up to 5 mm away (Fig. 2A). Responses at distances below 4 mm consist of an excitatory component followed by inhibition, while no responses are observed at greater distances. We also examined the spread of bursting activity over the disinhibited

network by disconnecting all interneurons and stimulating the leftmost 10 cells of the array with a 10 nA depolarizing current for 2 msec. The model exhibited a wavelike propagation of burst responses. The time the propagating activity reached a particular distance from the stimulus, was taken to be the moment the average AMPA-current over a block of ten cells, centered at that distance, became nonzero. The propagating velocity, calculated through a least squares fit to distance-time data, was ∼0.145 m/sec (Fig. 2B). Note that the size of the array was doubled to 2000 pyramidal cells in this simulation to get a better estimate of the propagation velocity. We also examined the influence on the propagation velocity of varying the extent of excitatory connections. We gradually increased $\sigma_{PY}$ from a range of 300 μm (30 cells) to 1.2 mm (120 cells) and each time repeated the above experiment (Fig. 2C). The propagation velocity increased along with the spread of excitatory connections, eventually reaching a plateau. The above features have also been observed in recordings in rat CA3 longitudinal slices and simulations of a more sophisticated CA3 computational model (Miles et al., 1988), and validate the connectivity scheme implemented here.

To examine the full CA3 model, we restored inhibition in the network and depolarized all pyramidal cells on their dendritic compartment by a current whose magnitude was Gaussian distributed over the population: $I = 0.3 \pm 0.03$ nA (mean ± SD). To increase the input heterogeneity, it was redrawn for every cell every 1 msec of the simulation. No current was applied to the interneurons. The whole CA3 network exhibited population oscillations that involved both pyramidal cells and interneurons (Fig. 2D). Bursts were initiated in nonspecific locations on the array and quickly spread throughout the whole network via recurrent excitatory connections. They were terminated by strong interneuronal inhibition and by the afterhyperpolarization of pyramidal cells. The population oscillation frequency was estimated, from the autocorrelation of the average membrane potential of the array (not shown), to be approximately 7.5 Hz, which lies within the theta frequency range (4–10 Hz). Membrane potentials of individual cells [Fig. 2D (ii,iii)] indicate that the pyramidal cells fire mostly in bursts but very rarely, without a clear rhythmicity. In contrast the interneurons fire in almost all cycles at high frequencies and skip cycles only if their neighboring pyramidal cells did not fire. The shape of synaptic events, seen through the membrane potentials, varies between cycles and the underlying population oscillation is not always apparent through inspection of individual pyramidal cell potentials. One needs to examine the interneuronal activity or the total raster plot to see the overall rhythmical activity. Similar population events and membrane potential characteristics were reported via field and an intracellular recordings of pyramidal cells in CA3 slices *in vitro* (Traub et al., 1989; Ellender et al., 2010) and simulations of a two-dimensional CA3 model (Traub et al., 1989). That pyramidal cells rarely contribute to a population burst (and only ∼27% of cells fire in a burst on average) is a result of the strong inhibition they receive. By removing interneurons, the model exhibits epileptiform bursts at much lower frequencies involving

all pyramidal cells (not shown), similar to what was shown in disinhibited CA3 slices *in vitro* (Ellender et al,. 2010).

Finally, to examine whether the oscillation frequency of the population bursts is bounded within the theta range or depends strongly on the applied current we plotted the f–I curve for various mean amplitudes of depolarizing current [Fig. 2D (iv)]. Each time, the standard deviation of the distributed currents was set to 10% of the mean. The frequency never dropped below the theta range and monotonically increased with increasing depolarization. Although for currents higher than $I = 0.8$ nA the frequency is already slightly above the theta range, the characteristics mentioned above are distorted, as all pyramidal cells burst in every cycle and exhibit a clear oscillation. Therefore the quasi-synchronous oscillatory bursts appear to be bounded within the theta frequency range.

## Gamma Oscillations in the CA1 Model

We targeted our CA1 model validation on reproducing functional properties of this hippocampal area, focusing specifically on gamma oscillations that have been extensively studied in CA1 (Traub et al., 1999a).

We first focused on the purely interneuronal network in CA1 by removing all excitatory interactions. Figure 3A (i) illustrates the model behavior when all interneurons are depolarized by a current $I = 0.3 \pm 0.003$ nA (mean ± SD) Gaussian distributed over the population and redrawn every 1 msec (the current's SD is lower than in the CA3 model because interneuronal firing depends very strongly on the current magnitude). The raster plot indicates that there is rhythmical activity with local synchrony but the network lacks an overall synchronous oscillation. The average membrane potential shows a noisy rhythmicity and its autocorrelation reveals a strong peak at 14 msec corresponding to a gamma oscillation of 71.43 Hz. When increasing the mean current tenfold (3 nA) with SD again at 1% of the mean (0.03 nA) the oscillation frequency increases beyond the gamma range, reaching approximately 167 Hz [Fig. 3A (ii)], which is within the ripple range. The overall synchrony appears to be much higher as the average membrane potential exhibits clear oscillations.

To quantify the network's overall synchrony we used the average coherence measure $\kappa(\tau)$ introduced by Wang and Buzsáki (1996), which ranges from 0 to 1, with 1 corresponding to total synchrony. After fixing the time window $\tau$ to $0.1/f$, where $f$ is the population frequency, $\kappa(\tau)$ was calculated to be approximately 0.022 for the first case but increased to about 0.112 for the second one, verifying that the population oscillations were much more synchronous at a frequency well beyond the gamma range.

The dependence of the oscillation frequency and the population synchrony on the magnitude of the applied current was examined by depolarizing the network with currents of increasing mean amplitudes. The current's SD was fixed at 1% of the mean. Figure 3A (iii) reveals an almost linear dependence of the frequency on the mean current. Moreover, the frequency does not drop below ˜40 Hz, indicating that the network can
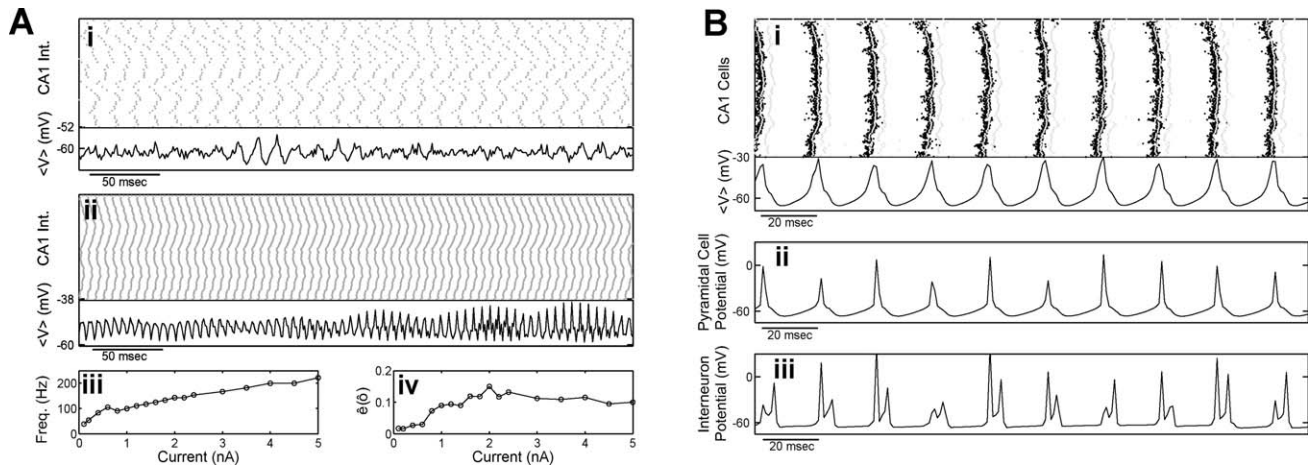
FIGURE 3.    A: Gamma oscillation in the CA1 interneuronal network, where pyramidal cells have been removed. All interneurons are depolarized by a current that is Gaussian-distributed over the network, with 0.3 ± 0.003 nA (mean ± SD) and is redrawn every 1 msec. The raster plot indicates weak local synchrony and the average membrane potential reveals a population oscillation of approximately 71.43 Hz, within the gamma frequency range (a). When the gaussian distributed current is increased to 3 ± 0.03 nA, a faster and more synchronous population oscillation emerges, with frequency 167 Hz, within the ripple range (b). Oscillation frequency (c) and average synchrony measure κ(τ) (d) as a function of the mean current. Note that the population synchrony is higher at frequencies above the gamma range. B: Raster plot of the whole CA1 model (pyramidal cells are shown in black and interneurons in gray) and average membrane potential of the whole array (a). The population oscillation is approximately 48 Hz with interneurons firing mostly in spike doublets with the first spike following the quasi-synchronous pyramidal spikes by 2 msec on average. Examples of membrane potentials from one pyramidal cell (b) and one interneuron (c).

only exhibit oscillations within the gamma range or above it. The coherence measure κ(τ) initially increases, reaching a peak for a mean current of 2 nA, beyond which it slowly drops, remaining at relatively high values even for corresponding frequencies above the ripple range [Fig. 3A (iv)]. As will be shown below for the full model (Fig. 11), this coherence at high frequencies depends strongly on the decay time of inhibition whereas the strength of inhibitory connections mainly affects the oscillation frequency. Note that, for all currents, the population frequencies are far below the range of frequencies (~100–400 Hz) that interneurons with the implemented heterogeneous intrinsic properties would fire at, if they were uncoupled and the same current was applied to them (Wang and Buzsáki, 1996).

We then restored excitatory connections and interneuron-to-pyramidal inhibition, and depolarized pyramidal cells by the same scheme that was used in the interneuronal network, with a mean current of 6 nA. No current was injected in the interneurons. The raster plot and the average membrane potential, shown in Figure 3B (i), illustrate a stable oscillatory activity, with pyramidal cells firing in synchrony and interneurons firing mostly in spike doublets, with an inter-spike interval of 3–4 msec. The first spike of the doublets follows the pyramidal spike by 2 msec on average. The autocorrelation of the average membrane potential has a peak at 21 msec, indicating that the oscillation frequency is roughly 48 Hz, which is again within the gamma range, although well below the range of frequencies exhibited by the interneuronal network for tenfold weaker current. Similar gamma oscillation characteristics have been seen *in vitro* in tetanically stimulated CA1 slices (Traub et al., 1996b; Whittington

et al., 1997) and in computational CA1 models (Traub et al., 1996b; Whittington et al., 1997; Traub et al., 1999b).

## SPWRs in the Full CA3-CA1 Model

We couple the two individual models through the Schaffer collaterals from CA3 to CA1. All pyramidal cells in CA3 are depolarized by implementing the same variable Gaussian-distributed current of 0.3 ± 0.03 nA as in Figure 2D. No external input is given to interneurons or CA1 cells.

Figure 4A illustrates the activity of the full model as depicted by the raster plots of both areas and the average membrane potential and total synaptic currents of all CA1 cells within the recording site. As before, the CA3 area exhibits theta-periodic population bursts that initiate in nonspecific locations and spread over the whole CA3 network. Each population burst produces a corresponding burst of activity in CA1 by exciting both pyramidal cells and interneurons through the Schaffer collaterals. Note that interneurons participate very strongly in the CA1 burst, causing the average membrane potential of the recording site to decrease significantly on every burst. The synaptic currents reveal a fast oscillatory activity during each burst. The individual membrane potentials of three random CA1 pyramidal cells and three interneurons (Fig. 4C,D) imply that although both pyramidal cells and interneurons receive strong excitation from CA3, only the latter fire almost on every burst and usually with a large number of spikes, while pyramidal cells fire rarely with mostly just one spike per cycle. Similar spiking characteristics have been observed in CA1 ripple recordings (Buzsáki et al., 1992; Ylinen et al., 1995; Csicsvari
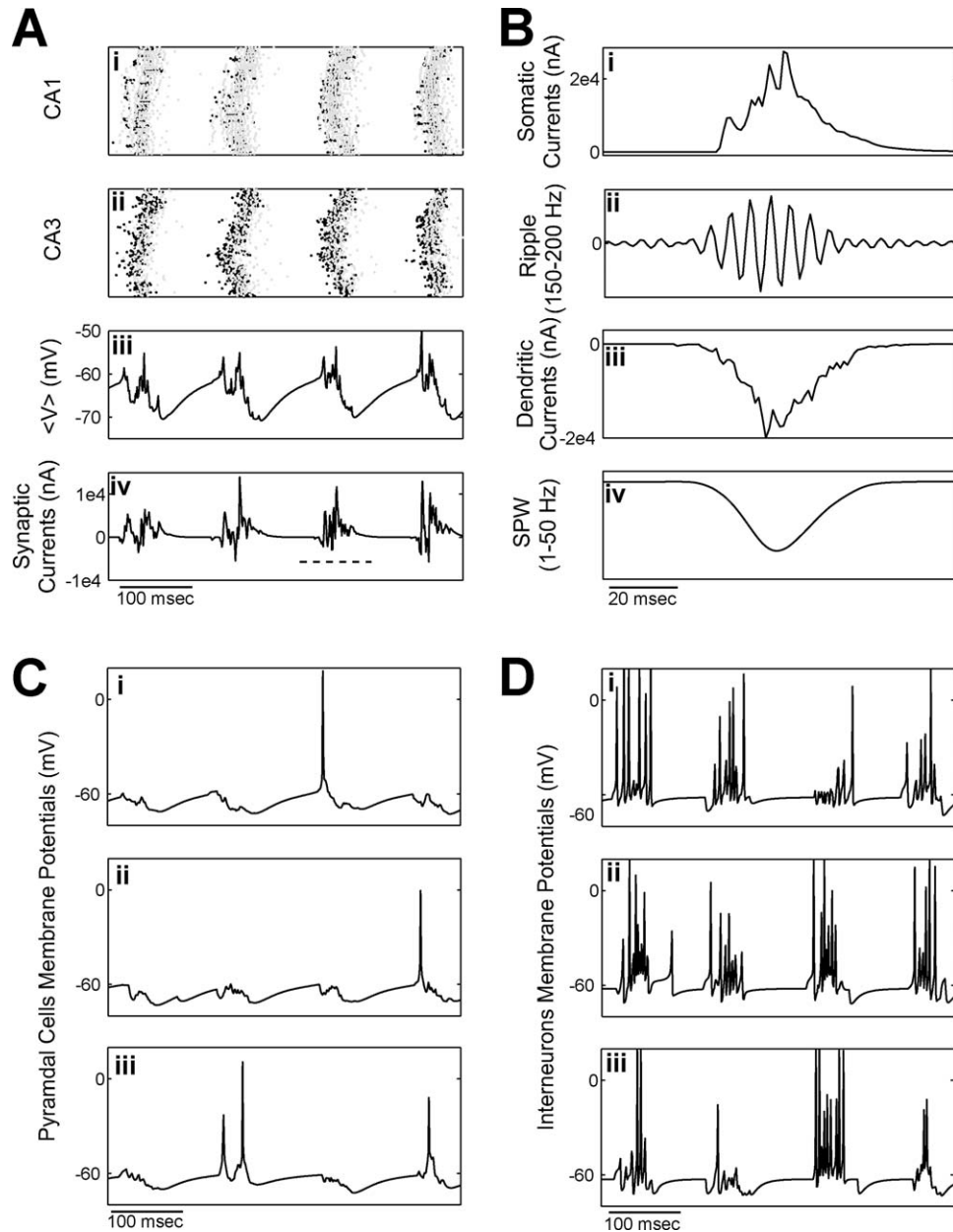
FIGURE 4.    A: Activity of the full CA3-CA1 model. Raster plot of the whole CA1 array (a), raster plot of the whole CA3 array (b, pyramidal cell spikes are shown in black and interneuronal in gray), average membrane potential (c) and total synaptic currents (d) of the 560 μm-long recording site in CA1. B: CA1 synaptic currents corresponding to the pyramidal cell layer (a) during the underlined burst and their 150–200 Hz bandpass filtered version (b). Schaffer collateral excitatory currents corresponding to the dendritic layer (c) and their 1–50 Hz lowpass filtered version (d). C, D: Membrane potentials from three CA1 pyramidal cells [C (a–c)] and three CA1 interneurons [D (a–c)].

et al., 1999). Finally both cell types show rich synaptic activity that fluctuates strongly with a very fast alteration between excitatory and inhibitory synaptic inputs.

To examine the activity in CA1 during an individual burst we zoom into one of them [underlined in Fig. 4A (iv)]. In Figure 4B, the total synaptic currents of the recording site were split into those corresponding to the dendritic layer and those corresponding to the pyramidal cell layer. Bandpass filtering the somatic currents in the 150–200 Hz frequency range [Fig. 4B (ii)] yields a clear ripple-like oscillatory pattern. Similarly, lowpass

filtering the dendritic currents in the 1–50 Hz range [Fig. 4B (ii)] yields a Sharp Wave curve that peaks in parallel with the ripple. This activity, exhibited by the model, closely resembles corresponding raw and filtered CA1 extracellular recordings during SPWRs (Buzsáki et al., 1992; Ylinen et al., 1995; Csicsvari et al., 1999; Klausberger et al., 2003; Maier et al., 2003).

The power spectral profile of the synaptic activity in the CA1 somatic layer was examined to ensure that the observed fast oscillatory modulation lies within the ~150–200 Hz ripple-frequency range. The spectrogram of the total synaptic
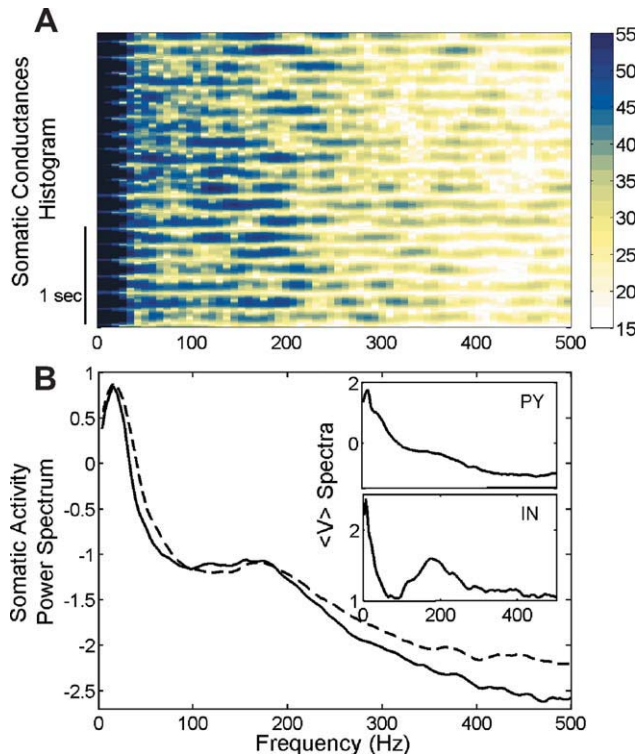
**FIGURE 5.** **A: Spectrogram of the total synaptic conductance over the recording site in the full CA3-CA1 model. Bands of high power at ripple frequencies are visible. B: Power spectrum of the total synaptic conductance (solid line) and the total synaptic currents (dashed line) in the site over a 30 sec-long simulation. Both measures were normalized by subtracting their means and dividing by their standard deviations. The strong theta-peaks are due to the theta-periodic recurrence of the input from the CA3 bursts. Insets: Power spectra of the average membrane potentials of pyramidal cells (top) and interneurons (bottom) in the recording site over the same simulation. [Color figure can be viewed in the online issue, which is available at wileyonlinelibrary.com.]**

conductance (Fig. 5A) reveals narrow bands of high power bounded in a range of frequencies that lie roughly around the ripple range but vary between cycles. Figure 5B contains the power spectrum of both the total synaptic conductance and total synaptic currents in the recording site over a 30 sec-long simulation. A clear peak appears in the spectral power of both measures around the ripple frequency range. The insets show the power spectra of the average membrane potential of pyramidal cells (top) and interneurons (bottom) in the recording site. The interneurons show a very clear intracellular ripple-frequency oscillation whereas the pyramidal cells exhibit a much less pronounced peak, suggesting the interneurons as a likely candidate for generating ripple oscillations.

We next examined correlations between spike activity and the average ripple. First we isolated all detected ripple events and calculated the average ripple as described in the Methods section. The spikes of all pyramidal cells and interneurons in the recorded site during each detected ripple were also aligned with its minimal point as reference (0 msec) and were superimposed on the average ripple (Fig. 6A). We calculated the spike

histogram for all cells, aligned with the average ripple (Fig. 6B,C). At this point we separated the pyramidal cells into two groups, those that receive many synapses for each Schaffer collateral connection and those that receive a close-to-average number or below. We arbitrarily set the threshold to 19.5 synapses per input connection (1.5 times the mean number of synapses per connection). The first group contains 32% of all pyramidal cells that are very excitable due to the stronger input they receive. The histograms of both groups are shown in Figure 6B (gray bars for the first group and black for the second). The interneuronal histogram (Fig. 6C) shows a very clear rhythmical spiking, with maximum activity phase locked to the negative half-wave of the average ripple, its peak slightly following the ripple's negative peak (1 msec). In the pyramidal cell histogram, the number of spikes is much lower, and the activity differs between the two cell groups. Specifically, cells that belong to the group with weaker excitation appear to have almost no ripple modularity in their firing. Most of their firing activity is concentrated on the beginning of the event, before significant synchronous inhibitory spiking begins. In contrast, the cells receiving stronger input exhibit clear rhythmical spiking similar to the interneurons. Their activity is also phase locked to the average ripple and its peak coincides with the ripple's negative peak, indicating that on average they fire slightly before the interneurons. Similar pyramidal and interneuronal phase lockings between spike activity and field ripples have been established through recordings (Buzsáki et al., 1992; Ylinen et al., 1995; Csicsvari et al., 1999).

The membrane potentials of all recorded cells during the detected ripples were also isolated, highpass filtered (40–500 Hz) to remove any slow components, and aligned with the minimum point of their corresponding ripple as reference. The average potentials of pyramidal cells and interneurons are plotted with the average field ripple in Figure 6D. It appears that the average pyramidal cell membrane potential (solid line) oscillates in phase with the interneuronal one (dashed line) during the ripples and they are both correlated with the interneuronal spike histogram. Consequently, they exhibit a small phase precession relative to the average field oscillation, with their peaks coinciding with the rising phase of the ripple, similar to intracellular potentials observed in anesthetized rats (Ylinen et al., 1995).

The histograms in Figure 6 support the idea that the ripple oscillation is actually a result of the interneuronal activity since only the few very pyramidal cells, receiving stronger input than average, manage to fire during a ripple episode. Figure 7A shows the percentage of the recorded pyramidal cells (solid line) and interneurons (dashed line) that fire on every ripple. Clearly all interneurons fire on almost every cycle, while the percentage of pyramidal cells that fire during an episode is 21.9% on average. Figure 7B shows that the percentage of ripples during which a pyramidal cell fires increases with the cell's excitability, quantified by the number of synapses it receives per connection. An almost linear relationship arises close to our implemented threshold between the two cell groups (solid line).
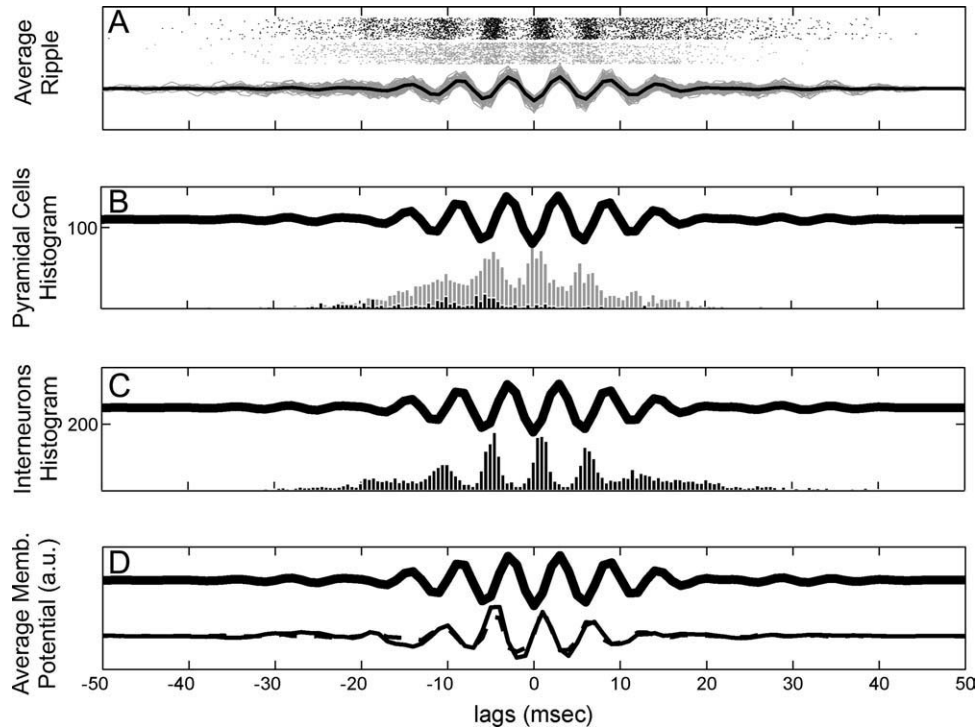
**FIGURE 6. Field oscillation correlation with unit firing and average membrane potential. A: All detected ripples (gray lines) are aligned according to their minimum point and the average ripple is drawn (thick black line). Spikes from pyramidal cells (gray) and interneurons (black) are aligned around the corresponding ripples. B: Spike histogram of pyramidal cells aligned with the average rip-ple. Pyramidal cells are split into two groups: The ones that receive more than 19.5 synapses for each Schaffer collateral connection (1.5 × the average 13, gray bars) and those that receive less than 19.5 (black bars). C: Interneuronal spike histogram. D: Average membrane potential of pyramidal cells (solid line) and interneurons (dashed line) aligned with the average ripple.**

The activity of an average cell during a ripple was studied by examining the synaptic input it receives and its resulting firing rate. Figure 8A depicts the average postsynaptic current from all types of synapses received by a cell during a ripple, averaged over all detected ripples and all relevant cells. All currents start to rise early during the ripple and peak along with the peak of the excitatory input from CA3 received by the average pyramidal cell (solid line) or interneuron (dashed line). The inhibitory
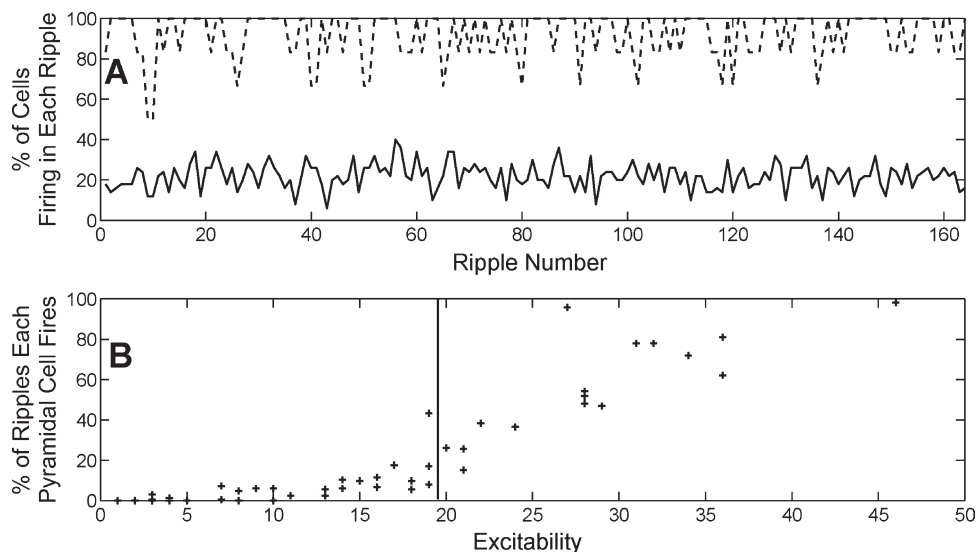


**FIGURE 7. A: Percentage of pyramidal cells (solid line) and interneurons (dashed line) that fire on each detected ripple. B: Percentage of ripples during which each pyramidal cell fires, versus the cell's excitability (as number of synapses it receives per CA3 incoming connection). The vertical line represents the thresh-old (19.5 synapses per CA3 incoming connection) between the two pyramidal cell groups.**
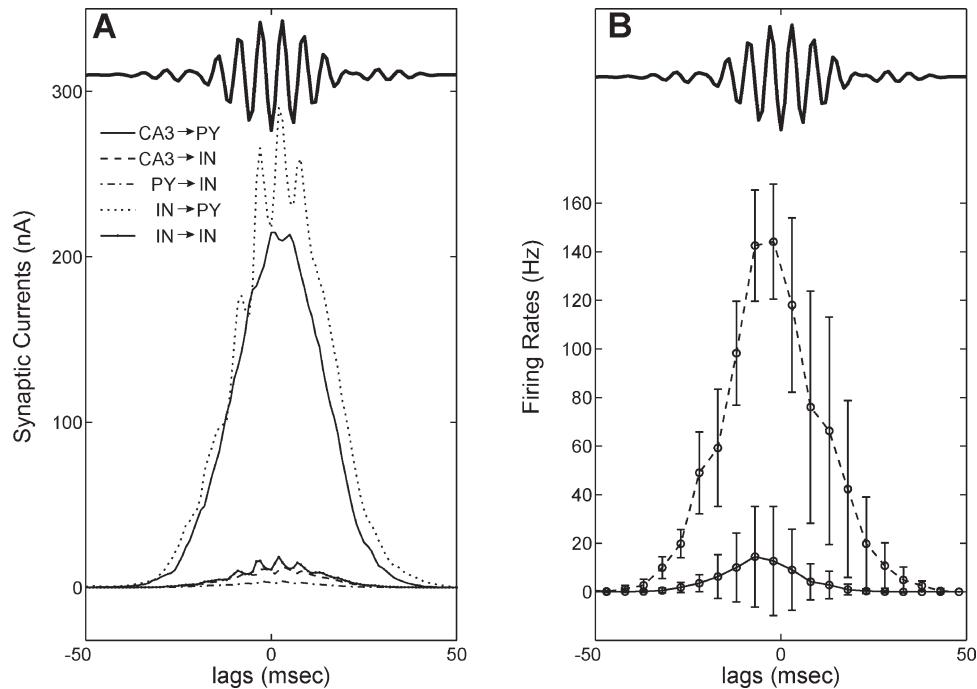
**FIGURE 8.** **A:** Postsynaptic currents received by a pyramidal cell or interneuron during an average ripple (thick line). The ripple power correlates with the rise of excitatory input a CA1 cell receives from CA3. Note the close balance between the excitation and inhibition a CA1 pyramidal cell receives during the ripple. The same holds for the average interneuron as well. **B:** Average firing rates of pyramidal cells (solid line) and interneurons (dashed line) in relation with the average ripple (thick line), calculated over 5 msec bins. Error bars correspond to the SD. The interneuronal rate is below the ripple frequency and both rates peak roughly 5 msec before the ripple's power peak (0 msec).

currents in both pyramidal cells and interneurons exhibit ripple oscillation phase locked to the average ripple with the same phase delay seen in Figure 6D. In contrast, excitatory inputs are much smoother and they appear to be in close balance with inhibitory inputs in both the average pyramidal cell and interneuron. Note that the average excitatory current an interneuron receives during a ripple, from both CA3 inputs and CA1 pyramidal cells, is ~3.7 nA. With a steady depolarizing current of this amplitude, an isolated noninhibited cell would fire with 400 Hz frequency (Wang and Buzsáki, 1996). The corresponding frequency for the purely inhibitory network would be 180 Hz [Fig. 3A (iii)], which is roughly in the middle of the ripple range.

The average firing rates in the recorded site are depicted in Figure 8B for both pyramidal cells (solid line) and interneurons (dashed line). They were calculated using 5 msec nonoverlapping bins. Interneuronal firing starts first and is sustained longer than the pyramidal, while both rates peak at roughly 5 msec before the ripple power peak (0 msec), in agreement with firing rates in Csicsvari et al. (1999, 2000). Most interestingly, the interneuronal rates barely reach the ripple frequency range, indicating that the ripple oscillation is an interneuronal population oscillation while the average interneuron fires at lower frequencies.

Another major characteristic of SPWRs is that they appear to be very synchronous throughout the hippocampus (Ylinen et al., 1995; Chrobak and Buzsáki, 1996). To check whether the ripples in our model are close to synchronous, we simultaneously recorded the total synaptic conductance from three more sites of the same length as the default (560 μm). The respective centers of two of them lay 300 μm away from that of the default recording site, and the center of the third site is 500 μm away. Figure 9A displays one example of the same ripple episode recorded from all four sites. The filtered total synaptic conductances appear to oscillate nearly synchronously throughout all four sites, with very small jitter, as was also seen for similar space scales in Ylinen et al. (1995). This synchrony is disrupted for larger distances of the order of several mm (not shown). We computed the average ripple on each site during the same 30 sec simulation, isolating the bandpass filtered data fragments from all sites that coincide with each detected ripple in the default site and aligning them with its minimum value. The averages from each site plotted along with the average ripple on the default site (Fig. 9B) appear to be coherent, with zero time lags between them. Therefore, averaging over a large number of events abolishes the jitter seen in individual ripples, again in agreement with Ylinen et al. (1995).

To ensure that CA1 ripples are not a direct consequence of a similar oscillation in CA3, we examined the correlation between the CA1 average ripple and the CA3 pyramidal cell firing. If the CA1 ripples are just a CA3 rhythm that travels through the Schaffer collaterals to CA1, similar correlations as those in Figure 6 should exist, with some phase difference due to the conductance delay of the Schaffer collaterals. Figure 10A
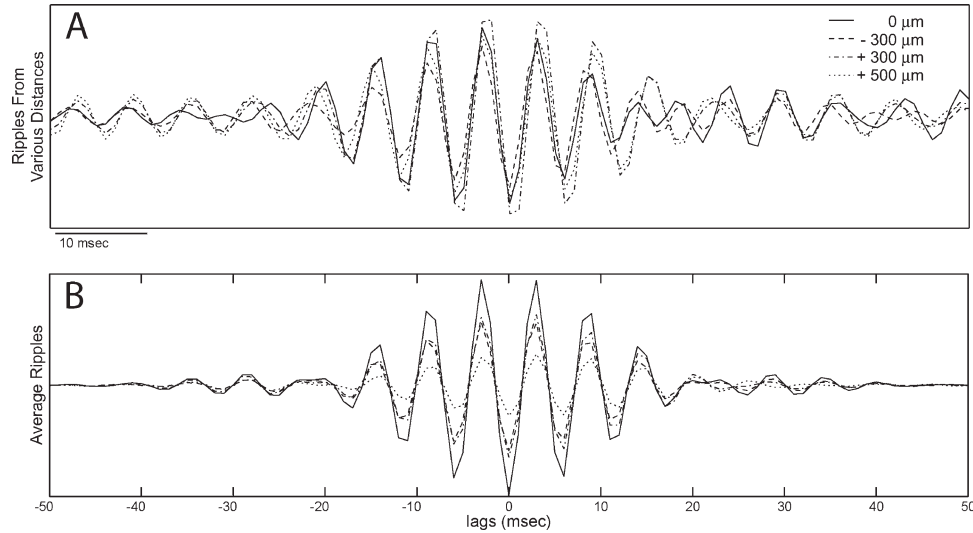
**FIGURE 9.** **Long range synchrony of ripple events in CA1. A: One ripple recorded simultaneously from four different sites: the default recording site (solid line), two sites lying 300 μm away** **from it (dashed and dashed dotted lines), and one lying 500 μm away (dotted line). B: Similar for the average ripple calculated from each site**

shows that this is not the case. In fact, there appears to be no ripple-like modularity in the firing of pyramidal cells in CA3, to correlate with CA1 activity. Note that we have taken all CA3 pyramidal cells into account here since the Schaffer collaterals are so widespread that a CA1 cell receives input from the majority of CA3 cells. Nevertheless similar results are acquired even if we take only the cells in the CA3 part of the array that corresponds to the CA1 recording site (not shown).

The varying frequency ranges of the power peaks in the spectrogram of Figure 5A, imply that the ~150–200 Hz range is not intrinsic in the CA1 model but depends on the input



**FIGURE 10.** **A: CA1 average ripple correlation with CA3 pyramidal cell firing histogram. Spikes from all CA3 pyramidal cells were included in the histogram. B: Mean firing rate of all CA1 pyramidal cells during each CA3 burst, plotted over the percentage of CA3 pyramidal cells that fired during the burst. An almost linear relation arises between the magnitude of a CA3 burst and the frequency of the CA1 response. The solid line is a least squares fit with a slope of 0.145.**

from CA3. This was verified by examining the relationship between the magnitude of CA3 bursts and the magnitude of CA1 responses. CA3 bursts were detected by a threshold equal to the SD of the RMS of the total synaptic currents recorded in the CA3 equivalent of the CA1 default site. The threshold for setting the burst limits was half the SD. The burst magnitude was quantified by the percentage of CA3 pyramidal cells that fired during the burst while the magnitude of CA1 responses was measured as the average firing rate of all pyramidal cells in CA1 during the burst. Plotting the CA1 responses over the extent of the corresponding CA3 bursts (Fig. 10B) reveals an overall monotonic relation, resembling qualitatively a corresponding relation seen in Csicsvari et al (2000). Similar results were found for the average firing rate of CA1 interneurons (not shown).
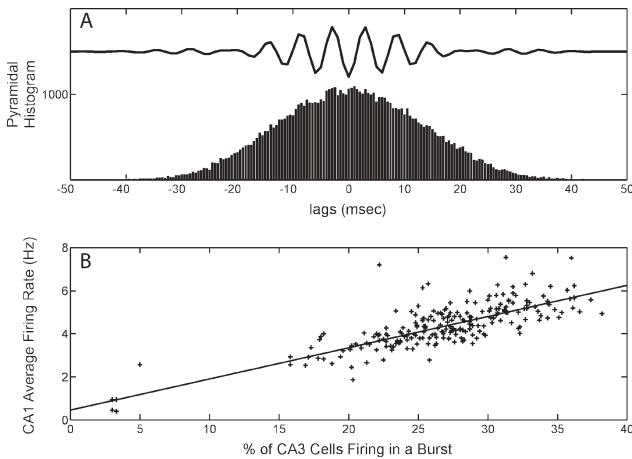
## The Role of Inhibition and Excitation in Ripples

The role of inhibition and excitation in CA1 on the generation and synchronization of ripples was studied by modifying the parameters of inhibitory and excitatory interactions. Parameters in CA3 were unaltered to retain the same input to CA1 as before.

We altered the strength of all inhibitory connections in CA1 by first reducing the maximum synaptic conductance $\bar{g}_{GABA}$ in Eq. (1) by 70%, setting $\bar{g}_{GABA} = 0.3$ nS, and then increasing it to $\bar{g}_{GABA} = 3$ nS. The same was done in another pair of simulations for excitatory connections, setting $g_{AMPA}$ to the previous two values respectively. We also examined the effect of the synaptic decay times by decreasing and increasing $\tau_{GABA}$ and $\tau_{AMPA}$ separately. Since $\tau_{GABA}$ is different for pyramidal cells and interneurons (7 msec and 2 msec, respectively) both values were altered accordingly. Each case was simulated for 30 sec. Figure 11 presents the power spectrum of the somatic

conductances for each case along with the default value case for comparison and excerpts of CA1 raster plots for the nondefault cases.

The effect of altering these parameters is partly reflected in the way the high-frequency peak (150–200 Hz) of the default spectral profile changes. For weaker inhibition the peak widens and shifts to higher frequencies (300 Hz) indicating that there is still some activity at ripple frequencies but on average the oscillations are much faster (Fig. 11A). The corresponding raster plot indicates that interneurons now fire at higher rates along with an increased pyramidal activity. On the contrary, stronger inhibition results in shifting a narrower peak to lower frequencies and the raster plot clearly shows weak interneuronal and pyramidal activity. Changing the inhibitory decay time has a different effect (Fig. 11B). For faster inhibition decay, spectral peaks are sustained but lie at higher frequencies ($\sim$250 Hz) as interneurons can now fire at much higher rates. Slower inhibition though does not shift the peak but instead just attenuates it, indicating the loss of coherent oscillations in some particular frequency range.

Changing the excitation strength affects the input all neurons receive from CA3 and the extra excitation of interneurons from nearby pyramidal cells. It has the opposite effect to that seen for $\bar{g}_{GABA}$ changes, with weaker (stronger) excitation decreasing (increasing) the oscillation. Similar results hold for the decay time with faster decay leading to slower oscillations and slower decay to faster ones (not shown).

In summary, changing the level of inhibition or excitation in the network, or even the decay time of excitation, alters mainly the oscillation frequency. On the other hand, prolonging the decay time of inhibition disrupts the population synchrony. Note that the same results hold for the ripple frequency oscillations of the purely interneuronal network of CA1, depicted in Figure 2A (b), another indication of the relatively small contribution of pyramidal firing in ripple generation.

# DISCUSSION

We presented here a CA3-CA1 network model of the corresponding two areas in the rat hippocampus along the longitudinal direction. The two CA models reproduce a series of neurophysiological observations related to anatomical features or functional properties of the two areas. They are coupled together in a Schaffer collateral-like manner with feedforward excitation from CA3 to CA1. We have shown that quasi-synchronous population bursts in the CA3 model evoke responses in the CA1 model that exhibit numerous characteristic features observed in real SPWRs.

## Model Architecture

Both models are relatively simple, one-dimensional, with similar architecture, parameter values and connectivity schemes, and single cell models that accurately capture the firing proper-

ties of the corresponding neurons, without any detailed cell anatomy. The main emphasis was on the implemented connectivity being physiologically realistic with connectivity extents and probabilities close to reported ones and synaptic strengths following reported PSPs (see Methods section).

Although a large variety of inhibitory cell types exists in the hippocampus (Freund and Buzsáki, 1996; Cutsuridis et al., 2010a,b), we only implemented fast somatic inhibition in the models. In addition to the obvious model simplification that this allows, this choice was based on the observation that, during SPWRs, different interneuronal types exhibit diverse behaviors, with only basket and bistratified cells increasing their discharges, while other interneurons stop spiking (Klausberger et al., 2003; Klausberger and Somogyi, 2008). Our model suggests that the increased activity of basket cells suffices to model many basic ripple characteristics. The mechanisms that generate such an unequal participation of interneuronal classes in ripples are beyond the scope of this work. The functional role of the different classes has been studied with detailed CA1 computational models in relation to memory encoding and retrieval (Cutsuridis et al., 2008, 2010a,b; Cutsuridis and Wennekers, 2009; Cutsuridis and Hasselmo, 2010).

Only fast synaptic interactions were implemented (AMPA and GABA$_A$) since pharmacological disruption of NMDA or GABA$_B$ receptors in CA1 did not affect SPWRs (Maier et al., 2003), implying that they are not involved in ripple generation. On the other hand application of the AMPA-receptor antagonist CNQX completely abolished ripples (Maier et al., 2003; Behrens et al., 2005; Wu et al., 2005). Our results support this observation since fast synaptic time scales appear to be key for ripple generation (Fig. 11B).

## The CA3 Model

Recordings have shown that when applying a stimulus to one end of a rat CA3 longitudinal slice, responses consisting of an excitatory component followed by inhibition can be recorded in the stratum pyramidale at distances within 5 mm from the stimulation (Miles et al., 1988). It has also been shown that when the stimulus is presented at one end of the longitudinal CA3 slice in which inhibition is blocked with picrotoxin, bursts propagate, without any decrease, in a wavelike fashion throughout the slice with an average propagation velocity of $0.14 \pm 0.04$ m/sec (Miles et al., 1988). Simulations with a spatially exponentially decaying recurrent connectivity revealed that the propagation velocity increases when increasing the spatial extent of these recurrent connections (Miles et al., 1988). All the above three features were successfully reproduced by our CA3 model (Fig. 2A–C), validating the implemented connectivity of the recurrent excitatory connections, the balance between excitation and inhibition and the physiologically driven choice of $\sigma_{PY} = 1$ mm which was important in getting the correct propagation velocity in the disinhibited array.

Similarly to intracellular recordings in CA3 slices *in vitro* (Traub et al., 1989; Ellender et al., 2010) and computational modeling (Traub et al., 1989) the full CA3 model produces
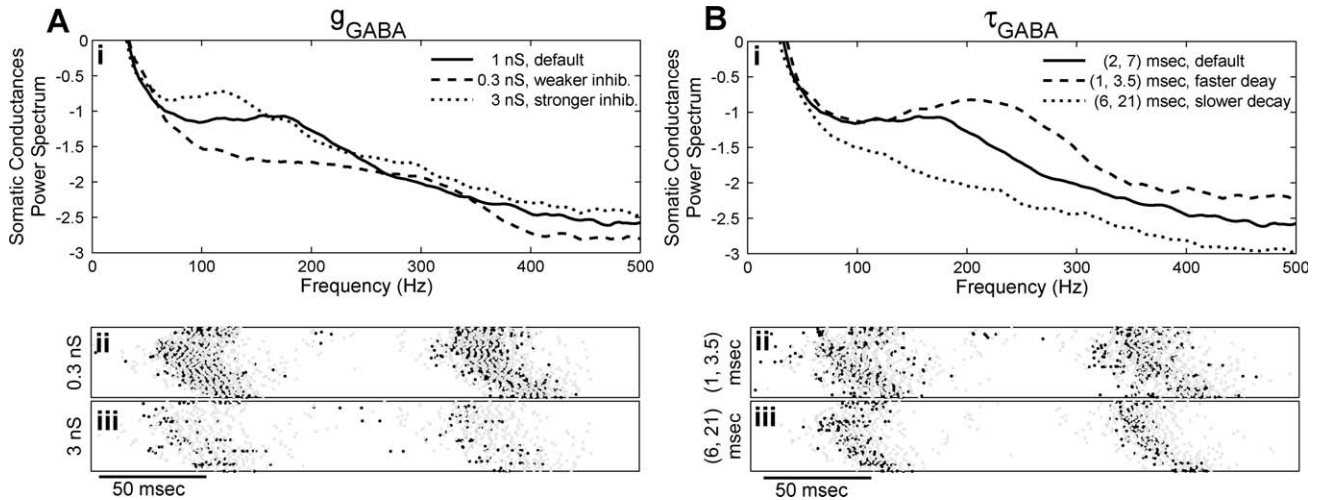
**FIGURE 11.    Comparison of CA1 somatic conductances power spectra between the default model and cases where the following synaptic parameters have been modified: A: the maximum unitary GABA conductance $g_{GABA}$, B: the decay time of inhibitory synaptic variables $\bar{g}_{GABA}$. Below each spectral profile, examples of CA1 raster plots from the two non-default cases are plotted and can be compared with Figure 4A (a). The parameter values in each case** are given in the figure legend. **Changes in the strength of inhibitory synapses alter mainly the oscillation frequency, while prolonging the decay time of inhibition disrupts synchronous oscillations in some particular frequency. Note that qualitatively same results hold for the ripple range oscillations of the purely interneuronal network of CA1.**

population bursts initiating at nonspecific sites and quickly propagating through recurrent excitation with pyramidal cells firing rarely during a population event and interneurons participating in every cycle with multiple spikes (Fig. 2D). Strong inhibition is necessary to keep the number of participating pyramidal cells low, thus increasing the recurrence frequency of the bursts by decreasing the overall after hyperpolarization in the network. The theta frequency range (4–10 Hz) occurrence of these population bursts is not to be confused with the classical theta oscillations in the hippocampus during wakefulness or REM sleep described and studied extensively elsewhere (for an extensive review see Buzsáki, 2006). Moreover, all cells receive a variety of excitatory and inhibitory synaptic inputs in each population burst, unlike in CA3 slices *in vitro* where their synaptic input is almost exclusively inhibitory (Ellender et al., 2010). This inconsistency could be due to severing of long range excitatory connections in the slice preparation that diminishes the effect of excitatory interactions, which could also explain the small spatial extent of the bursts in slices (Ellender et al., 2010) unlike in our model where each population burst travels throughout the whole network. In the context of this work, the quasi-synchronous bursts serve as an extensive depolarizing input to CA1 in the full model that can generate SPWRs.

We can thus conclude that our simplistic one-dimensional CA3 model is able to reproduce, with sufficient accuracy, various characteristics and behaviors seen in experimental recordings and simulations of a much more complex two-dimensional CA3 model (Traub and Miles, 1991). Note that various features of CA3 circuits such as transduction probabilities, PSP rise times, synaptic depression or facilitation (Andersen et al.,

2006) have not been included in the model. For example it has been estimated that the single-spike-transduction probability in a pyramidal-pyramidal connection is 5% but the burst-transduction probability can rise up to 50% (Traub and Miles, 1991). In our model, neither a single EPSP nor a burst can cause a postsynaptic pyramidal cell to fire. Nevertheless such features appear not to be necessary for the simulation of the functional and anatomical features presented here.

## The CA1 Model

Interneuronal gamma oscillations have been detected in the CA1 region *in vitro* under tetanic stimulation, in the presence of glutamate receptor blockers (Whittington et al., 1995). This and other studies indicated that transient gamma oscillations can rely solely on GABA-mediated inhibition, with fast somatic inhibition, namely basket cells, being the most likely candidate for generating and sustaining such oscillations (Bartos et al., 2007). Moreover, various computational models of inhibitory networks reproduced gamma oscillations, usually assuming slow and weak inhibition and homogeneous or global network connectivity (Traub et al., 1996a; Wang and Buzsáki, 1996; Whittington et al., 1997; White et al., 1998). The population synchronization in such models was shown to be sensitive to heterogeneities in connectivity and in the driving current and changes in the synaptic strength and kinetics (Wang and Buzsáki, 1996; White et al., 1998). Even slight inhomogeneities or a limited spatial spread of connections can shift the network from global synchrony to local (Traub et al., 1999a). This very limited spatial synchrony is also encountered in our CA1 inhibitory network during gamma oscillations. Tonic depolarization,

albeit with a noisy component, short-range heterogeneous connectivity and noisy intrinsic cell parameters do not allow an overall synchronization of firing during the oscillations [Fig. 3A (i)].

This sensitivity to heterogeneity could be ameliorated to some extent by incorporating fast, strong, shunting inhibition along with synaptic delays (Bartos et al., 2002, 2007). Though lacking shunting inhibition, synchrony is enhanced in our network by incorporating multiple connections between neighboring interneuronal pairs, with strong and fast decaying IPSPs along with axonal delays. In fact, axonal conductance delays were crucial, since, by removing them, any synchrony of oscillations was completely abolished (not shown). The importance of incorporating long synaptic delays, longer than the inhibitory decay time, in establishing fast synchronous interneuronal oscillations has been shown through mathematical and computational analysis in a similar set up (Brunel and Wang, 2003). In our model, the conductance delay between two connected interneurons can be longer than the decay time, reaching up to 3 msec (0.1 mm/msec conductance velocity with connections reaching out to ˜300 μm, Table 2), thus aiding the oscillation synchrony.

Although the frequency of the population oscillations does not drop below the gamma range, with stronger depolarization it reaches the ripple frequency range. The model reproduced the linear relationship between the applied current amplitude and the oscillation frequency [Fig. 3A (iii,iv)] seen in other inhibitory network simulations (Traub et al., 1996a; Wang and Buzsáki, 1996). Interestingly, we found that global synchrony is considerably stronger at those higher frequencies, with cells firing in a clear rhythmical pattern [Fig. 3A (ii)]. A similar relationship between synchrony at ripple frequencies and the external drive was reported in simulations of interneuronal networks with global random connectivity and fixed delays (Brunel and Wang, 2003). As shown in Figure 11B, synchrony at such high frequencies depends strongly on the small decay time of inhibition. The condition for this time constant to be smaller than ∼5 msec for synchronous oscillations at ∼200 Hz to occur, was shown through mathematical analysis and computational modelling of heterogeneous interneuronal networks (Chow et al., 1998; White et al., 1998). It appears that even with our scheme of spatially restricted connectivity and distance-dependent delays, a similar condition and synchrony-drive dependence still hold. Note that our unusual choice of 2 msec for the decay time is based on recent electrophysiological studies which report similar GABA$_A$ time constants in CA1 (Bartos et al, 2002, 2007).

When depolarizing the pyramidal cells in the full CA1 model they fired synchronously followed by interneuronal spike doublets (Fig. 3B). The network oscillated, still within the gamma range, but at considerably lower frequencies than the interneuronal ones, even though the applied current was much stronger. The frequency decrease is a result of the extra delays introduced by long range excitation in the pyramidal-interneuron-pyramidal loop of the full network (Brunel and Wang, 2003). Similar characteristics of gamma oscillations have also

been seen *in vitro* in electrophysiological recordings from tetanically stimulated CA1 slices (Traub et al., 1996b; Whittington et al., 1997) and have been reproduced in computational models with a simplistic chain-like architecture (Traub et al., 1996b; Whittington et al., 1997) or more realistic two-dimensional connectivity (Traub et al., 1999b). In these recordings, when the stimulation was performed simultaneously on two sites 4 mm apart, very tightly synchronized transient gamma oscillations appeared in both sites after a short latent period. This long range synchrony that extended several millimeters consisted of pyramidal cells firing single spikes and interneurons firing mostly spike doublets with the first spike being in phase with the pyramidal spikes (Traub et al., 1996b; Whittington et al., 1997). Doublets, along with long range synchrony, would disappear when the network was stimulated only locally implying that doublet firing is a result of the increased excitation the interneurons received due to the long-range axonal connections of further away pyramidal cells (Traub et al., 1996b; Whittington et al., 1997). These results led to the suggestion that doublet firing is the necessary driving mechanism for long range synchrony of gamma oscillations in CA1 [for a qualitative analysis see (Traub et al., 1999a)] which was also demonstrated with analytical methods (Ermentrout and Kopell, 1998). It has been shown that for gamma oscillations in a network with long range nonrecurrent excitation and local inhibition, doublets would arise when the first interneuronal spike was generated by local excitatory input whereas the second one by the delayed input from more distant cells. The resulting inhibition determines the time of the next spike of nearby pyramidal cells and consequently the next oscillatory cycle. Under this regime, the network undergoes synchronous oscillations, robust to mild heterogeneities (Ermentrout and Kopell, 1998). In our model, the lag between the pyramidal spikes and the two spikes of the doublets (2 and 5–6 msec respectively) implies that the first spike is due to excitatory input from local cells at distances within $\sigma_{PY}$ whereas the second one is from distant cells up to $3\sigma_{PY}$ away, verifying the above analysis.

The ratio of excitation to inhibition and the synaptic delays are important in this mechanism (Ermentrout and Kopell, 1998; Brunel and Wang, 2003). Specifically, removing conductance delays, either excitatory or inhibitory, completely abolished any oscillations. Moreover, if pyramidal-to-interneuron excitation is not strong enough to evoke doublets, or if feedback inhibition is not strong enough to time the next firing of pyramidal cells, then long range synchrony can not be sustained. In support of this, administration of AMPA-receptor antagonists (Whittington et al., 1997) or GABA-blocking morphine (Whittington et al., 1998) to CA1 slices disrupts long-range synchrony of the oscillations. Reducing the unitary AMPA- or GABA-conductance in our model by 75% abolished long-range oscillations as well, although some gamma rhythmicity persisted in the former case and small clusters of locally synchronous oscillations still existed out of phase, (also reported by Traub et al., 1999a). The fact that our full CA1 model reproduces these features indicates a correct balance between inhibition and excitation in the network. Yet, contrary to oscillations of

the purely inhibitory network, the gamma oscillations in the full CA1 model are not directly related to the ripple mechanism since pyramidal firing is very sparse in ripples.

## SPWRs in the Full CA3-CA1 Model

Sharp waves, observed in the dendritic layer in CA1, are thought to be strong depolarizations of the cell dendrites arising from population bursts in CA3 and reaching CA1 through the Schaffer collaterals. We thus coupled the two individual models in a full CA3-CA1 network, via feed forward Schaffer collateral-like connections in an effort to examine whether the quasi-synchronous bursts in the CA3 model would trigger a response in CA1 that resembles sharp waves and a simultaneous fast synchronous oscillation in the somatic layer with ripple characteristics.

CA1 responded to the strong input with intense synaptic activity on fast time scales involving both excitatory and inhibitory populations (Fig. 4A,B) with characteristics very similar to SPWRs from extracellular recordings in CA1 (Buzsáki et al., 1992; Ylinen et al., 1995; Csicsvari et al., 1999; Klausberger et al., 2003; Maier et al., 2003). Note that the sharp waves in the model do not show a small inhibitory component after the negative peak (Buzsáki, 1986; Buzsáki et al., 1992). Perhaps this after hyperpolarization component is caused by dendritic inhibition, which is omitted in the model. It could also be due to somatic inhibition captured by dendritic-layer recordings. Spectral analysis of synaptic activity in the CA1 somatic layer revealed a clear peak around 150–200 Hz (Fig. 5), similar to spectral profiles in Buzsáki et al. (1992), Maier et al. (2003) and Both et al. (2008), verifying that on average the CA1 somatic fast oscillations were indeed within the ripple frequency range.

Interestingly, the high frequency of the ripple oscillations was not reflected in the spiking activity of individual neurons. Membrane potentials of pyramidal cells showed that they fired extremely rarely during a ripple, and mostly with a single spike, while interneurons were much more active, firing in every episode with a large number of spikes (Fig. 4C,D). These features are characteristic of CA1 recordings during ripple activity (Buzsáki et al., 1992; Ylinen et al., 1995; Csicsvari et al., 1999) and hint at the interneurons as the driving force in ripple oscillations. Indeed, average firing rates during ripple episodes showed that interneurons begin spiking earlier and their firing lasts longer than pyramidal cells (Fig. 8B), seen also in Csicsvari et al. (1999, 2000). This conclusion is also supported by the clear modularity and phase locking of the interneuronal firing histogram to the negative half wave of the average ripple (Fig. 6C). Nevertheless, firing rates were on average below the 150–200 Hz band, implying that ripples are an overall population oscillation, not an effect of the average firing of individual interneurons. In short, the external drive from CA3 produces synchronous ripple-frequency oscillations of the CA1 interneuronal network in the model, similar to those in Figure 3A (b), only now cells can skip cycles due to heterogeneities in the input and recurrent inhibition.

Pyramidal cells, embedded in the strong background interneuronal oscillation, spike much more rarely, mostly right before the interneurons, resulting in a phase locking of their spiking to the negative peak of the ripple on the onset of the inhibitory barrage. These phase correlations are also established via intracellular and extracellular recordings (Buzsáki et al., 1992; Ylinen et al., 1995; Csicsvari et al., 1999; Klausberger et al., 2003). In the model, only the cells receiving stronger input from CA3 can synchronize their firing with the overall field oscillation. The rest get too strongly inhibited to show rhythmical activity and fire randomly mainly in the beginning of the ripple episode, before the peak of interneuronal firing (Figs. 6B and 7B). Therefore, the excitatory spikes come mostly from a minority of pyramidal cells, which fire on many more ripples than the rest. Specifically, only about 22% of pyramidal cells fired on average during a ripple (Fig. 7A). This feature agrees with extracellular recordings where approximately only 10% of all recorded pyramidal cells participated in an average ripple with some cells participating in up to 40% of successive episodes and others fire very rarely (Ylinen et al., 1995).

At the peak of the CA3 input, interneuronal activity reaches its maximum intensity, reducing further both pyramidal and inhibitory spikes. This is reflected in the average firing rates which peak ∼5 msec before the ripple peak (Fig. 8B), again in agreement with a similar time difference (5–10 msec) seen in average rates from extracellular recordings (J. Csicsvari, personal communication).

Average membrane potentials of both cell types appear to be in phase with the interneuronal spike histogram, exhibiting a similar small phase shift compared to the average extracellular ripple, with their peaks coinciding with the rising portions of the ripple waves (Fig. 6D). This phase difference is also seen in intracellular recordings from anesthetized rats (Ylinen et al., 1995), and is probably due to the slow interneuronal conduction velocities. Inhibitory postsynaptic conductances (which constitute the vast majority of postsynaptic activity within CA1, Fig. 8A) appear to lag behind spikes and membrane potentials by ˜2 msec. The time lag corresponds to a distance of 200 μm or $2\sigma_{IN}$ of inhibitory synaptic inputs from interneuronal spikes, which would imply that the delay is mostly due to the time it takes for inhibition to reach cells lying further than distance $\sigma_{IN}$ from an average interneuron. The delay indicates the importance of using the synaptic conductance as a measure of the extracellular synaptic activity, particularly in fine time-scale studies. Processing synaptic currents instead, which contain the membrane potential in their definition [Eq. (1)], will result in an average ripple that is slightly shifted backward in relation to the spikes. This will artificially produce a similar phase difference between the field oscillation and the unit firing (with pyramidal cells firing during the rising phase of the ripple and interneurons firing at its peaks), which contradicts the aforementioned phase lockings seen in recordings.

The fact that the fast oscillations were generated within CA1, and were not contained within the CA3 input, was shown by the lack of any correlation between CA3 firing and CA1 oscillations (Fig. 10A). According to our simulations, the

actual frequency range of the ripples is not an intrinsic property of the CA1 circuit architecture but a direct result of the magnitude of the excitatory input from CA3. Due to the variability in the magnitude of CA3 bursts, the frequency range also varies, with a clear relationship between the number of CA3 pyramidal cells firing during a burst episode and the mean firing rate of CA1 pyramidal cells during the evoked response (Fig. 10B). A similar relationship between these two measures was reported through extracellular recordings (Csicsvari et al., 2000) and implies that the more extensive and synchronous a CA3 burst is, the higher the frequency of the field oscillation. This is also supported by the shift in the spectral ripple-peak when excitation parameters are altered, with stronger or more slowly decaying EPSPs leading to higher frequency oscillations (not shown). According to this dependence of the ripple frequency on the magnitude of the Schaffer collateral input, the model predicts that an *in vitro* partial cut of Schaffer collateral axons in a longitudinal CA3-CA1 slice would decrease the observed ripple oscillation frequency.

Finally, note that SPWRs have also been reported in CA3 slices *in vitro* (Maier et al., 2003; Ellender et al., 2010). In our CA3 model, although the population bursts may account for sharp waves, ripples are absent. This is probably due to the lack of recurrent inhibition in the model. The inclusion of CA1-like connections between CA3 interneurons with an anatomically realistic connectivity scheme, in a future version of the model, could synchronize inhibitory firing and potentially generate ripple oscillations in CA3 as well. Moreover, we expect that long range excitation is reduced in CA3 slices making the connectivity more similar to CA1, which may help explain the generation of ripple-like oscillations in the slices.

## Pharmacological Effects on Ripples

An important factor in the mechanism of ripple generation appears to be the relation between excitation and inhibition in the CA1 network. The postsynaptic currents generated on the average cell during ripples reveal a tight balance between a smooth excitatory input from CA3 and a fast-oscillating inhibition (Fig. 8A). The average interneuron receives enough excitation to fire at frequencies twice as fast as ripples, but cross-inhibition retains the interneuronal network within ripple frequency range. A disruption of this sensitive balance has a corresponding effect on the ensuing oscillation frequency, shifting the spectral peak to different frequency ranges (Fig. 11).

This balance disruption can be induced pharmacologically by various anesthetics. Ketamine for example has no significant effect on AMPA excitation (only depresses NMDA receptors which are not relevant to SPWRs) but enhances $GABA_A$ inhibition (Krasowski and Harrison, 1999; Rudolph and Antkowiak, 2004). According to Figure 11A, this inhibition enhancement would shift the oscillations to lower frequencies. A similar inhibition enhancement in CA3 would further diminish the excitatory input to CA1, reducing the frequency further. This shift is in agreement with the observation that population oscillations dropped to 90–150 Hz, in *in vivo*

extracellular recordings on ketamine-anesthetized rats (Ylinen et al., 1995).

The opposite shift, to higher frequencies, occurs when the inhibition-to-excitation ratio is decreased, although ripple-range frequencies still have significant power, even when IPSP amplitudes are reduced by 70% (Fig. 11A). This is supported by recordings on CA1 minislices *in vitro* under the $GABA_A$ receptor antagonist gabazine, where ~200 Hz ripple oscillations persisted to some degree (Nimmrich et al., 2005). The reduction of IPSP amplitudes under 0.3 μm of gabazine was roughly 70%, similar to our corresponding simulation with $\bar{g}_{GABA} = 0.3$ nS. It is noteworthy that, in CA3-CA1 slices administered with bicuculline and gabazine, abolishing $GABA_A$ inhibition, ripples were replaced by large epileptiform bursts that still carried a ~200 Hz oscillation component (Maier et al., 2003).

Moreover, fast synaptic time scales are also crucial, with faster decay times leading to faster oscillations, while with slower IPSP decay times, the oscillations do not become slower but rather get attenuated overall (Fig. 11B). The importance of fast decay inhibition could be linked with reported effects on ripples of the gap junction-blocker anesthetic halothane. Halothane has been shown to disrupt CA1 ripple activity in *in vivo* recordings of anesthetized rats (Ylinen et al., 1995). Under deep halothane-induced anaesthesia, irregular sharp wave activity was maintained but 200 Hz oscillations were almost completely abolished. Other gap junction blockers (carbenoxolone and octanol) had similar effects in CA1 minislices *in vitro*, reducing the frequency of spontaneous sharp wave occurrence and even more so that of ripple activity (Maier et al., 2003). This has led to the suggestion that gap junctions are a key factor in the SPWR mechanism, since they can yield fast and synchronous oscillations. Nevertheless, gap junction blockers are quite nonspecific, affecting chemical synapses as well. Specifically, halothane has a combined effect on both chemical excitation and inhibition (Nishikawa and MacIver, 2000), depressing glutamate-mediated synaptic EPSP responses in both pyramidal cells and interneurons (Perouansky et al., 1995, 1996; Kirson et al., 1998), in combination with an approximately 2.5-fold prolongation of $GABA_A$ IPSP decay time (Gage and Robertson, 1985; Nishikawa and MacIver, 2000). A similar prolongation of $\tau_{GABA}$ in our model also resulted in severe attenuation of the ripple spectral peak indicating the loss of any particular high frequency oscillation (Fig. 11B). The effect would be even stronger with the combined reduced excitation in CA3, shifting oscillations to even lower frequencies. Thus the model suggests that halothane effects on chemical synapses alone could explain the loss of ripple-like oscillations.

## SPWRs and Memory Consolidation

Another very important feature of SPWRs is that they exhibit long range synchrony over the whole longitudinal extent of both CA areas (Ylinen et al., 1995; Chrobak and Buzsáki, 1996). In fact SPWRs extend to the rat subicular complex and even the enthorinal cortex, involving the synchronized participation of tens of thousands of cells (Chrobak and Buzsáki,

1996). Individual ripples, recorded simultaneously with multi-site probes 300 µm apart along the longitudinal CA1 axis, show a very small jitter between them (1 msec) but on average their time lag drops to zero (Ylinen et al., 1995). Synchrony over such space scales of hundreds of µm is successfully reproduced by our model (Fig. 9). Apart from the wide distribution of the Schaffer collaterals, which induce a homogeneity in the input from CA3, this synchrony appears to be induced mainly by the recurrent inhibition in CA1 which locks the inhibitory spikes in global oscillations and is enhanced by the interneuronal phase resetting caused by sparse firing of nearby pyramidal cells, as was also suggested in Ylinen et al. (1995). Nevertheless, synchrony is disrupted in larger space scales of several mm (not shown).

The strong transient output that is produced during such massive population discharges is very likely to affect cortical targets, making SPWRs a possible vehicle for transferring neuronal information from the hippocampus to the neocortex for long-term storage, during deep stages of sleep. Various studies of the correlations between hippocampal ripples and slow oscillations in the cortex during deep sleep provide further support for the role of ripples in memory (Siapas and Wilson, 1998; Sirota et al., 2003; Battaglia et al., 2004; Isomura et al., 2006).

One basic assumption of the model is that interneurons receive direct excitation by Schaffer collaterals. The model can produce similar SPWRs without such an input to interneurons, with all excitation coming from their neighboring pyramidal cells. Nevertheless, this set up would abolish the particular group of pyramidal cells that discharge during ripples and would result in all pyramidal cells firing in every cycle of the ripple before evoking interneuronal firing. This contradicts the observation of very sparse pyramidal firing (Ylinen et al., 1995; Csicsvari et al., 1999, 2000) and interneuronal discharge rising before the pyramidal (Csicsvari et al., 1999, 2000). Most importantly, it would contradict the fact that neuronal participation in ripples is not random, with only a particular subset of pyramidal cells discharging during most ripple episodes (Ylinen et al., 1995).

The heterogeneity in the response of CA1 pyramidal cells to the CA3 input was implemented through variability in the number of synapses Schaffer collaterals make on each cell. The small number of cells that fire during ripples, receive many more synapses per incoming connection than average, and can be thought of as representing neurons in the rat CA1 that are targeted by a larger portion of CA3 or receive stronger EPSPs than average. Although such a highly excitable subset is necessary in the model for reproducing the selective participation reported in Ylinen et al. (1995), its existence in the rat CA1 area has not yet been established. Nevertheless, we believe it supports the memory consolidation scenario since the cell subset appears to be formed by pre-existing experiences. Specifically, correlated discharges of rat hippocampal pyramidal cells during sleep have been shown to reflect the correlated activity of the same cells during earlier spatial exploration (Wilson and McNaughton, 1994). In fact the actual temporal sequences of those cells during wakeful training are preserved during sleep

(Skaggs and McNaughton, 1996) but replayed at faster time-scales during the short window of SPWRs, in the same order (Lee and Wilson, 2002) or reversed (Foster and Wilson, 2006; Diba and Buzsáki, 2007), [for an extensive discussion of the possible role of SPWRs in memory consolidation see Buzsáki (2006)].

In support of these observations, the subset of participating neurons in the model, instead of being implemented a priori, could emerge intrinsically in CA1 through a combination of repetitive firing of highly correlated CA3 cells and synaptic plasticity of the Schaffer collateral outputs. By implementing ensembles of strongly connected neurons in CA3, representing correlated place cells, the spontaneous CA3 population bursts could trigger their sequential firing and in combination with synaptic plasticity could potentiate synapses with their targeted CA1 cells. These CA1 cells would eventually form the strongly-driven subset, firing during ripples. A similar enhancement of single CA1 pyramidal cells' participation in ripples was found after their long-term potentiating stimulation (King et al., 1999). The replay of temporal patterns of the correlated CA3 ensemble during a burst would perhaps form a similar temporal pattern in CA1 and the whole process could take place either in a forward or reversed direction, shedding light to the bidirectional replay mechanism of place cell patterns observed during SPWRs (Diba and Buzsáki, 2007). Changing the correlated CA3 ensembles would eventually change the CA1 subset. Such a scheme would provide computational support to the observed SPWR generation in CA1 after long-term potentiation inducing stimulation of CA3 (Behrens et al, 2005) and even the place selective firing of CA1 cells in SPWRs during exploration (O'Neill et al, 2006). Coupling of such an extended model with a cortical network model in a feedback loop could help the study of temporal pattern transfer to the neocortex for long-term storage and the correlations between SPWRs and cortical slow oscillations (Siapas and Wilson, 1998; Sirota et al., 2003; Isomura et al., 2006). However, the model suggests that, in a situation where such a subset in CA1 is abolished, pyramidal spiking during ripples would be almost terminated, without severely affecting any other ripple characteristics (frequency, synchrony etc).

## Gap Junctions

Networks of axo-axonal gap junctions between pairs of pyramidal cells have been argued to underlie synchronous high-frequency oscillations in the hippocampus (Draguhn et al., 1998; Schmitz et al., 2001), rendering such electrically coupled networks a possible candidate for generating ripples. Indeed, CA1 models based on sparse axo-axonal gap junction connectivity give rise to fast 200 Hz populations oscillations even in the absence of chemical synapses (Traub et al., 1999b; Traub and Bibbig, 2000). Nevertheless, the lack of SPWR generation from antidromic stimulation of CA1 pyramidal axons and their preservation after removal of the distal part of these axons (Both et al., 2008) suggests that axo-axonal gap junctions may not be necessary for SPWRs.

Our model offers a different approach to the ripple generation mechanism that relies on inhibitory activity and solely on chemical synaptic interactions, avoiding the need for gap junctions. Since the model manages to reproduce a large number of basic SPWR characteristics and offers an interpretation of such characteristics within the context of a specific mechanism, we propose that gap junctions are not a necessary driving component for the SPWRs but rather an additional mechanism that helps the overall ripple generation. Such an "aiding" role of axo-axonal gap junctions is also hinted by the fact that SPWRs were not eliminated in mice lacking gap junction protein Cx36, only their frequency of occurrence decreased (Maier et al., 2002). Most importantly, gap junctions between pyramidal cell axons could serve as the mechanism for long range fast synchrony of the ripples in spatial scales of many mm. The future inclusion of an underlying gap junction network between pyramidal cells in our CA1 model would help the study of such a long-range synchronizing mechanism.

## A Proposed Mechanism for SPWRs

In summary, our simulation results, combined with the discussed neurophysiological findings, lead us to formulate a mechanism for the generation of SPWRs that is based purely on chemical synaptic interactions between excitatory and inhibitory populations. The proposed mechanism can be summarized by the following steps:

- CA3 quasi-synchronous population bursts produce a strong depolarizing input to both pyramidal cells and interneurons in CA1. The large number of outgoing connections from each CA3 pyramidal cell and their wide spatial extent helps render this input more homogeneous throughout CA1.
- Strong excitatory AMPA-synaptic currents generated in the dendrites of both cell types during the CA3 input produce a sharp wave in the dendritic layer of CA1.
- Fast spiking interneurons, such as the basket cells modeled here, get directly depolarized by the CA3 input, enough to intrinsically start spiking in a large range of high frequencies (100–400 Hz).
- The strong recurrent inhibitory connectivity in combination with the fast timescales of IPSPs, confines interneurons in a particular frequency range of roughly 150–200 Hz, which varies with the extent of the CA3 burst, and helps synchronize their membrane oscillations within a range of hundreds of μm. Recurrent inhibition also causes interneurons to skip cycles within the ripple resulting in a firing rate which is lower than the average membrane potential oscillation frequency of interneurons.
- Pyramidal cells have a much more passive role during the ripple episode. The strong inhibitory barrage they receive during the synchronous interneuronal firing cancels on average the depolarization from CA3. As a result they rarely manage to fire. Their sparse spikes appear mostly just before the interneuronal barrage and increase even further the depolarization of neighboring interneurons, helping enhance the population synchrony.

- A minority of pyramidal cells, which receives more CA3 input than average, manages to overcome the vast inhibition and produces the majority of pyramidal spikes in most events.
- The termination of the CA3 burst results in the consequent termination of CA1 activity. Interneurons continue to fire for a short amount of time due to delayed input from distant CA3 pyramidal cells.

## Acknowledgments

## REFERENCES

Ali AB, Deuchars J, Pawelzik H, Thomson AM. 1998. CA1 pyramidal to basket and bistratified cell EPSPs: Dual intracellular recordings in rat hippocampal slices. J Physiol 507:201–217.

Andersen P, Morris R, Amaral D, Bliss T, O'Keefe J. 2006. The hippocampus book. Oxford University Press, New York, USA.

Bartos M, Vida I, Frotscher M, Geiger JRP, Jonas P. 2001. Rapid signaling at inhibitory synapses in a dentate gyrus interneuron network. J Neurosci 21:2687–2698.

Bartos M, Vida I, Frotscher M, Meyer A, Monyer H, Geiger JRP, Jonas P. 2002. Fast synaptic inhibition promotes synchronized gamma oscillations in hippocampal interneuron networks. Proc Natl Acad Sci USA 99:13222–13227.

Bartos M, Vida I, Jonas P. 2007. Synaptic mechanisms of synchronized gamma oscillations in inhibitory interneuron networks. Nat Rev Neurosci 8:45–56.

Battaglia FP, Sutherland GR, McNaughton BL. 2004. Hippocampal sharp wave bursts coincide with neocortical "up-state" transitions. Learn Memory 11:697–704.

Behrens CJ, van den Boom LP, de Hoz L, Friedman A, Heinemann U. 2005. Induction of sharp wave–ripple complexes in vitro and reorganization of hippocampal networks. Nat Neurosci 8:1560–1567.

Bernard C, Wheal HV. 1994. Model of local connectivity patterns in CA3 and CA1 areas of the hippocampus. Hippocampus 4:497–529.

Both M, Bähner F, Halbach OB, Draguhn A. 2008. Propagation of specific network patterns through the mouse hippocampus. Hippocampus 18:899–908.

Brunel N, Wang XJ. 2003. What determines the frequency of fast network oscillations with irregular neural discharges? I. Synaptic dynamics and excitation-inhibition balance. J Neurophysiol 90:415–430.

Buhl EH, Halasy K, Somogyi P. 1994. Diverse sources of hippocampal unitary inhibitory postsynaptic potentials and the number of synaptic release sites. Nature 368:823–828.

Buhl EH, Cobb SR, Halasy K, Somogyi P. 1995. Properties of unitary IPSPs evoked by anatomically identified basket cells in the rat hippocampus. Eur J Neurosci 7:1989–2004.

Buzsáki G. 1986. Hippocampal sharp waves: their origin and significance. Brain Res 398:242–252.

Buzsáki G. 2006. Rhythms of the Brain. Oxford University Press.

Buzsáki G, Horvath Z, Urioste R, Hetke J, Wise K. 1992. High-frequency network oscillation in the hippocampus. Science 256:1025–1027.

Cannon RC, Wheal HV, Turner DA. 1999. Dendrites of classes of hippocampal neurons differ in structural complexity and branching patterns. J Comp Neurol 413:619–633.

Chow CC, White JA, Ritt J, Kopell N. 1998. Frequency control in synchronized networks of inhibitory neurons. J Comp Neurosci 5:407–420.

Chrobak JJ, Buzsáki G. 1996. High-frequency oscillations in the output networks of the hippocampal-entorhinal axis of the freely behaving rat. J Neurosci 16:3056–3066.

Cobb SR, Halasy K, Vida I, Nyiri G, Tamas G, Buhl EH, Somogyi P. 1997. Synaptic effects of identified interneurons innervating both interneurons and pyramidal cells in the rat hippocampus. Neuroscience 79:629–648.

Compte A, Sanchez-Vives MV, McCormick DA, Wang XJ. 2003. Cellular and network mechanisms of slow oscillatory activity (< 1 Hz) and wave propagations in a cortical network model. J Neurophysiol 89:2707–2725.

Csicsvari J, Hirase H, Czurko A, Mamiya A, Buzsáki G. 1999. Oscillatory coupling of hippocampal pyramidal cells and interneurons in the behaving rat. J Neurosci 19:274–287.

Csicsvari J, Hirase H, Mamiya A, Buzsáki G. 2000. Ensemble patterns of hippocampal CA3-CA1 neurons during sharp wave–associated population events. Neuron 28:585–594.

Cutsuridis V, Wennekers T. 2009. Hippocampus, microcircuits and associative memory. Neural Networks 22:1120–1128.

Cutsuridis V, Hasselmo M. 2010. Dynamics and Function of a CA1 Model of the Hippocampus during Theta and Ripples. In: Diamantaras K, Duch W, Iliadis LS, editors. Artificial Neural Networks-ICANN 2010, Part I, LNCS 6352. Springer-Verlag, Berlin, Germany, pp 230–240.

Cutsuridis V, Cobb S, Graham BP. 2008. Encoding and retrieval in a CA1 microcircuit model of the hippocampus. Artificial Neural Networks-ICANN 2008238–247.

Cutsuridis V, Cobb S, Graham BP. 2010a. Encoding and retrieval in a model of the hippocampal CA1 microcircuit. Hippocampus 20:423–446.

Cutsuridis V, Graham BP, Cobb S, Vida I. 2010b. Hippocampal Microcircuits: A Computational Modeler's Resource Book. Springer-Verlag, Berlin, USA.

Deuchars J, Thomson AM. 1996. CA1 pyramid-pyramid connections in rat hippocampus in vitro: dual intracellular recordings with biocytin filling. Neuroscience 74:1009–1018.

Diba K, Buzsáki G. 2007. Forward and reverse hippocampal place-cell sequences during ripples. Nat Neurosci 10:1241–1242.

Draguhn A, Traub RD, Schmitz D, Jefferys JGR. 1998. Electrical coupling underlies high-frequency oscillations in the hippocampus in vitro. Nature 394:189–192.

Ellender TJ, Nissen W, Colgin LL, Mann EO, Paulsen O. 2010. Priming of hippocampal population bursts by individual perisomatic-targeting interneurons. J Neurosci 30:5979–5991.

Ermentrout GB, Kopell N. 1998. Fine structure of neural spiking and synchronization in the presence of conduction delays. Proc Natl Acad Sci USA 95:1259–1264.

Foster DJ, Wilson MA. 2006. Reverse replay of behavioural sequences in hippocampal place cells during the awake state. Nature 440:680–683.

Freund TF, Buzsáki G. 1996. Interneurons of the hippocampus. Hippocampus 6:347–470.

Gage PW, Robertson B. 1985. Prolongation of inhibitory postsynaptic currents by pentobarbitone, halothane and ketamine in CA1 pyramidal cells in rat hippocampus. Brit J Pharmacol 85:675–681.

Geiger JRP, Melcher T, Koh DS, Sakmann B, Seeburg PH, Jonas P, Monyer H. 1995. Relative abundance of subunit mRNAs determines gating and Ca2+ permeability of AMPA receptors in principal neurons and interneurons in rat CNS. Neuron 15:193–204.

Goodman D, Brette R. 2008. Brian: a simulator for spiking neural networks in Python. Front Neuroinform 5:2 doi: 20.3389/neuro.11.005.2008.

Gulyás AI, Miles R, Sik A, Tóth K, Tamamaki N, Freund TF. 1993a. Hippocampal pyramidal cells excite inhibitory neurons through a single release site. Nature 366:683–687.

Gulyás AI, Mlles R, Hájos N, Freund TF. 1993b. Precision and variability in postsynaptic target selection of inhibitory cells in the hippocampal CA3 region. Eur J Neurosci 5:1729–1751.

Isomura Y, Sirota A, Özen S, Montgomery S, Mizuseki K, Henze DA, Buzsáki G. 2006. Integration and segregation of activity in entorhinal-hippocampal subregions by neocortical slow oscillations. Neuron 52:871–882.

King C, Henze DA, Leinekugel X, Buzsáki G. 1999. Hebbian modification of a hippocampal population pattern in the rat. J Physiol 521:159–167.

Kirson ED, Yaari Y, Perouansky M. 1998. Presynaptic and postsynaptic actions of halothane at glutamatergic synapses in the mouse hippocampus. Brit J Pharmacol 124:1607–1614.

Klausberger T, Somogyi P. 2008. Neuronal diversity and temporal dynamics: the unity of hippocampal circuit operations. Science 321:53–57.

Klausberger T, Magill PJ, Márton LF, Roberts JDB, Cobden PM, Buzsáki G, Somogyi P. 2003. Brain-state-and cell-type-specific firing of hippocampal interneurons in vivo. Nature 421:844–848.

Knowles WD, Schwartzkroin PA. 1981. Local circuit synaptic interactions in hippocampal brain slices. J Neurosci 1:318–322.

Krasowski MD, Harrison NL. 1999. General anaesthetic actions on ligand-gated ion channels. Cell Mol Life Sci 55:1278–1303.

Lanthorn T, Storm J, Andersen P. 1984. Current-to-frequency transduction in CA1 hippocampal pyramidal cells: slow prepotentials dominate the primary range firing. Exper Brain Res 53:431–443.

Lee AK, Wilson MA. 2002. Memory of sequential experience in the hippocampus during slow wave sleep. Neuron 36:1183–1194.

Li XJ, Somogyi P, Ylinen A, Buzsáki G. 1994. The hippocampal CA3 network: an in vivo intracellular labeling study. J Comp Neurol 339:181–208.

MacVicar BA, Dudek FE. 1980. Local synaptic circuits in rat hippocampus: interactions between pyramidal cells. Brain Res 184:220–223.

Madison DV, Nicoll RA. 1984. Control of the repetitive discharge of rat CA1 pyramidal neurones in vitro. J Physiol 354:319–331.

Maier N, Guldenagel M, Sohl G, Siegmund H, Willecke K, Draguhn A. 2002. Reduction of high-frequency network oscillations (ripples) and pathological network discharges in hippocampal slices from connexin 36-deficient mice. J Physiol 541:521–528.

Maier N, Nimmrich V, Draguhn A. 2003. Cellular and network mechanisms underlying spontaneous sharp waveripple complexes in mouse hippocampal slices. J Physiol 550:873–887.

Miles R. 1990. Synaptic excitation of inhibitory cells by single CA3 hippocampal pyramidal cells of the guinea-pig in vitro. J Physiol 428:61–77.

Miles R, Wong RK. 1986. Excitatory synaptic interactions between CA3 neurones in the guinea-pig hippocampus. J Physiol 373:397–418.

Miles R, Wong RK. 1987. Inhibitory control of local excitatory circuits in the guinea-pig hippocampus. J Physiol 388:611–629.

Miles R, Traub RD, Wong RK. 1988. Spread of synchronous firing in longitudinal slices from the CA3 region of the hippocampus. J Neurophysiol 60:1481–1496.

Miles R, Tóth K, Gulyás AI, Hájos N, Freund TF. 1996. Differences between somatic and dendritic inhibition in the hippocampus. Neuron 16:815–824.

Nimmrich V, Maier N, Schmitz D, Draguhn A. 2005. Induced sharp wave-ripple complexes in the absence of synaptic inhibition in mouse hippocampal slices. J Physiol 563:663–670.

Nishikawa K, MacIver MB. 2000. Membrane and synaptic actions of halothane on rat hippocampal pyramidal neurons and inhibitory interneurons. J Neurosci 20:5915–5923.

O'Neill J, Senior T, Csicsvari J. 2006. Place-selective firing of CA1 pyramidal cells during sharp wave/ripple network patterns in exploratory behavior. Neuron 49:143–155.

Perouansky M, Baranov D, Salman M, Yaari Y. 1995. Effects of halothane on glutamate receptor-mediated excitatory postsynaptic currents: A patch-clamp study in adult mouse hippocampal slices. Anesthesiology 83:109–119.

Perouansky M, Kirson ED, Yaari Y. 1996. Halothane blocks synaptic excitation of inhibitory interneurons. Anesthesiology 85:1431–1438.

Pinsky PF, Rinzel J. 1994. Intrinsic and network rhythmogenesis in a reduced Traub model for CA3 neurons. J Comp Neurosci 1:39–60.

Rudolph U, Antkowiak B. 2004. Molecular and neuronal substrates for general anaesthetics. Nat Rev Neurosci 5:709–720.

Salin PA, Prince DA. 1996. Electrophysiological mapping of GABAA receptor-mediated inhibition in adult rat somatosensory cortex. J Neurophysiol 75:1589–1600.

Sayer RJ, Friedlander MJ, Redman SJ. 1990. The time course and amplitude of EPSPs evoked at synapses between pairs of CA3/CA1 neurons in the hippocampal slice. J Neurosci 10:826–836.

Schmitz D, Schuchmann S, Fisahn A, Draguhn A, Buhl EH, Petrasch-Parwez E, Dermietzel R, Heinemann U, Traub RD. 2001. Axo-axonal coupling a novel mechanism for ultrafast neuronal communication. Neuron 31:831–840.

Siapas AG, Wilson MA. 1998. Coordinated interactions between hippocampal ripples and cortical spindles during slow-wave sleep. Neuron 21:1123–1128.

Sik A, Tamamaki N, Freund TF. 1993. Complete axon arborization of a single CA3 pyramidal cell in the rat hippocampus, and its relationship with postsynaptic parvalbumin-containing interneurons. Eur J Neurosci 5:1719–1728.

Sik A, Penttonen M, Ylinen A, Buzsáki G. 1995. Hippocampal CA1 interneurons: an in vivo intracellular labeling study. J Neurosci 15:6651–6665.

Sirota A, Csicsvari J, Buhl D, Buzsáki G. 2003. Communication between neocortex and hippocampus during sleep in rodents. Proc Natl Acad Sci USA 100:2065–2069.

Skaggs WE, McNaughton BL. 1996. Replay of neuronal firing sequences in rat hippocampus during sleep following spatial experience. Science 271:1870–1873.

Sorra KE, Harris KM. 1993. Occurrence and three-dimensional structure of multiple synapses between individual radiatum axons and their target pyramidal cells in hippocampal area CA1. J Neurosci 13:3736–3748.

Traub RD, Miles R. 1991. Neuronal networks of the hippocampus. Cambridge University, Press, New York, USA.

Traub RD, Bibbig A. 2000. A model of high-frequency ripples in the hippocampus based on synaptic coupling plus axon-axon gap junctions between pyramidal neurons. J Neurosci 20:2086–2093.

Traub RD, Miles R, Wong RK. 1989. Model of the origin of rhythmic population oscillations in the hippocampal slice. Science 243:1319–1325.

Traub RD, Miles R, Buzsáki G. 1992. Computer simulation of carbachol-driven rhythmic population oscillations in the CA3 region of the in vitro rat hippocampus. J Physiol 451:653–672.

Traub RD, Whittington MA, Colling SB, Buzsáki G, Jefferys JG. 1996a. Analysis of gamma rhythms in the rat hippocampus in vitro and in vivo. J Physiol 493:471–484.

Traub RD, Whittington MA, Stanford IM, Jefferys JG. 1996b. A mechanism for generation of long-range synchronous fast oscillations in the cortex. Nature 383:621–624.

Traub RD, Jefferys JG, Whittington MA. 1999a. Fast oscillations in cortical circuits. The MIT Press, Cambridge, Messachusetts, USA.

Traub RD, Schmitz D, Jefferys JG, Draguhn A. 1999b. High-frequency population oscillations are predicted to occur in hippocampal pyramidal neuronal networks interconnected by axoaxonal gap junctions. Neuroscience 92:407–426.

Traub RD, Whittington MA, Buhl EH, Jefferys JG, Faulkner HJ. 1999c. On the mechanism of the gamma right-arrow beta frequency shift in neuronal oscillations induced in rat hippocampal slices by tetanic stimulation. J Neurosci 19:1088–1105.

Wang XJ, Buzsáki G. 1996. Gamma oscillation by synaptic inhibition in a hippocampal interneuronal network model. J Neurosci 16:6402–6413.

White JA, Chow CC, Rit J, Soto-Trevino C, Kopell N. 1998. Synchronization and oscillatory dynamics in heterogeneous, mutually inhibited neurons. J Comp Neurosci 5:5–16.

Whittington MA, Traub RD, Jefferys JG. 1995. Synchronized oscillations in interneuron networks driven by metabotropic glutamate receptor activation. Nature 373:612–615.

Whittington MA, Stanford IM, Colling SB, Jefferys JG, Traub RD. 1997. Spatiotemporal patterns of gamma frequency oscillations tetanically induced in the rat hippocampal slice. J Physiol 502:591–607.

Whittington MA, Traub RD, Faulkner HJ, Jefferys JGR, Chettiar K. 1998. Morphine disrupts long-range synchrony of gamma oscillations in hippocampal slices. Proc Natl Acad Sci USA 95:5807–5811.

Wilson MA, McNaughton BL. 1994. Reactivation of hippocampal ensemble memories during sleep. Science 265:676–679.

Wu C, Asl MN, Gillis J, Skinner FK, Zhang L. 2005. An in vitro model of hippocampal sharp waves: regional initiation and intracellular correlates. J Neurophysiol 94:741–753.

Ylinen A, Bragin A, Nadasdy Z, Jando G, Szabo I, Sik A, Buzsáki G. 1995. Sharp wave-associated high-frequency oscillation (200 Hz) in the intact hippocampus: network and intracellular mechanisms. J Neurosci 15:30–46.